
Article:
Zhang, Y., Bai, J., Guo, K. et al. (9 more authors) (2024) An alloying strategy for tuning magnetism, thermal hysteresis, and mechanical properties in Ni-Mn-Sn-based Heusler alloys. Journal of Alloys and Compounds, 979. 173593. ISSN 0925-8388

https://doi.org/10.1016/j.jallcom.2024.173593

An alloying strategy for tuning magnetism, thermal hysteresis, and mechanical properties in Ni-Mn-Sn-based Heusler alloys

Yu Zhang [a,b], Jing Bai [a,b,d,*], Keliang Guo [a,b], Dan Liu [a,b], Jianglong Gu [c], Nicola Morley [d,*], Qingshuang Ma [b], Qiuzhi Gao [b], Yudong Zhang [e], Claude Esling [e], Xiang Zhao [a], Liang Zuo [a]

[a] Key Laboratory for Anisotropy and Texture of Materials (Ministry of Education), School of Material Science and Engineering, Northeastern University, Shenyang 110819, China

[b] Key Laboratory of Dielectric and Electrolyte Functional Material Hebei Province, School of Resources and Materials, Northeastern University at Qinhuangdao, Qinhuangdao 066004, PR China

[c] State Key Laboratory of Metastable Materials Science and Technology, Yanshan University, Qinhuangdao 066004, China

[d] Department of Material Science and Engineering, University of Sheffield, Sheffield, S1 3JD, UK

[e] Laboratoire d'Étude des Microstructures et de Mécanique des Matériaux, UMR 7239, LEM3, CNRS, University of Lorraine, 57045 Metz, France

*Corresponding author: Jing Bai: baijing@neuq.edu.cn

Nicola Morley: n.a.morley@sheffield.ac.uk

Abstract

Ni-Mn-Sn metamagnetic shape memory alloys have great application potential, with numerous advantages but are constrained by limitations, such as limited magnetization differences ($\triangle M$), large thermal hysteresis ($\triangle T_{Hys}$), and intrinsic brittleness. To ameliorate these limitations, fourth-element doping has been extensively experimentally conducted, yet theoretical insights at the atomic scale remain limited. Here, the phase stability, martensite transformation, magnetism, and mechanical properties of the $Ni_2Mn_{1.5}Sn_{0.5}$ alloy doped with a 3*d*-transition element *Z* (*Z* = Fe, Co, and Cu) were systematically investigated using the first-principles calculations, provide theoretical explanations for changes in physical properties. The phase transformation path and magnetic properties of Ni-Mn-Sn-*Z* alloys containing four-layered orthorhombic (4O) martensite were revealed. The strong ferromagnetic coupling between Ni-Co and the change in Mn_{Sn} magnetic moment spin direction are the primary reasons for the increase in austenite magnetic moment in $Ni_{2-x}Co_xMn_{1.5}Sn_{0.5}$ ($x > 0.125$) alloys. Cu doping leads to a reduction in volume contraction ($\triangle$V), thereby lowering $\triangle T_{Hys}$. The mechanical property results indicate that Fe or Cu doping significantly enhances the plasticity and

toughness, while Co doping reduces the toughness and increases stiffness. Furthermore, the origin of physical properties related to martensitic transformation and magnetism is explained by the electronic density of states. This research provides essential theoretical explanations for understanding and predicting the changes in physical properties associated with different doping elements, which is critical for the design and development of high-performance Heusler alloys.

Keywords: Ni-Mn-Sn, First-principles calculations, Modulated martensite, Martensitic transformation, Magnetic and mechanical properties

1 Introduction

Heusler-type Ni-Mn-*X* (*X* = In, Sn, and Sb) metamagnetic shape memory alloys (MSMAs) possess the intriguing ability to concurrently change the crystal structure and magnetization during the phase transformation[1-4], which has lead to researchers exploring their related magneto-controlled functional behaviors, e.g., magnetic field-induced strain (MFIS)[5,6], magnetocaloric effect (MCE)[7,8], and magnetoresistance (MR)[9,10]. Thus, these alloys have great potential to be developed as materials for various applications, such as high-performance sensors, actuators, and environmentally friendly solid-state refrigerants. Notably, the cost-effectiveness of the Ni-Mn-Sn alloys compared to the Ni-Mn-Ga and Ni-Mn-In alloys enhances their competitiveness in application fields.

The stoichiometric Ni_2MnSn alloy does not undergo a martensitic transformation. Theoretical and experimental results prove that martensitic transformation exclusively occurs when $x \geq 0.36$ by adjusting the Mn/Sn ratio in the $Ni_2Mn_{1+x}Sn_{1-x}$ alloys[1,11]. From the perspective of developing high-performance functional materials, the $Ni_2Mn_{1+x}Sn_{1-x}$ alloys not only need to undergo martensitic transformation, but also must overcome other limitations, such as the low magnetization of the high-temperature austenite results in limited magnetization difference, significant thermal hysteresis, and intrinsic brittleness. Therefore, numerous experiments have used 3*d*-transition elements, specifically Fe, Co, and Cu, to dope ternary Ni-Mn-Sn alloys, to improve these properties.

Researchers found that Fe-doped Ni-Mn-Sn alloys can significantly improve the mechanical properties of the alloys while achieving good MCE and elastocaloric effects (eCE). Zhu *et al*. observed that the $Ni_{41}Fe_3Mn_{46}Sn_{10}$ alloy displayed both excellent cyclic stability after 200 stress cycles and an adiabatic temperature change of -10.3 K under a stress of 350 MPa[12]. The strength and

ductility of the $Ni_{51.5}Mn_{34}Fe_6Sn_{8.5}$ alloy can reach 2000 MPa and 21% respectively[13]. Zhang *et al*.[14] found that the $Ni_{47-x}Mn_{43}Sn_{10}Co_x$ alloys with Co substituted for Ni increased the magnetization of austenite from 13.5 $A\cdot m^2/kg$ with Co free to 91.7 $A\cdot m^2/kg$ with x = 6, and obtained a remarkable magnetic entropy change ΔS_M = 29.5 J/kg·K under a magnetic field 5 T. A noteworthy MCE with a ΔS_M of 19.1 J/kg·K can be observed in the $Ni_{43}Mn_{46-x}Co_xSn_{11}$ (x = 5) alloy under the magnetic field of 1 T[15]. Cu alloying can effectively increase the yield strength and reduce the $\triangle T_{Hys}$, and can also obtain good MCE and eCE[16-19]. The $\triangle T_{Hys}$ of the $Ni_{47}Mn_{40}Sn_{13-x}Cu_x$ alloys decreases from 18 K at x = 0 to 13 K at x = 1, and ΔS_M increases from 7.5 to 15.6 J/kg·K[20]. The $Ni_{44}Mn_{41}Sn_{11}Cu_4$ alloy can achieve an adiabatic temperature change of -8 K under a transformation strain of 1.3%[21]. The above results demonstrate that the substitutions of Fe, Co, and Cu at specific sites in the Ni-Mn-Sn alloys can help the alloys meet the expected requirements. Nevertheless, there exists an insufficiency in delving into the underlying physical mechanisms that underpin the observed experimental results.

It is well known that the twin boundary movement resistance of non-modulated (NM) martensite is significantly higher than that of modulated martensite, as well as the ferromagnetic ordering of modulated martensite, resulting in large MFIS in the alloys[22-24]. Therefore, researchers anticipate that alloys can undergo two-step or even multi-step martensite transformation instead of direct transformation from austenite to NM martensite. Extensive experimental studies have revealed the presence of intermediate modulated martensite 4O martensite when the fourth element is doped with components near the $Ni_{50}Mn_{37.5}Sn_{12.5}$ ($Ni_2Mn_{1.5}Sn_{0.5}$) alloy as the matrix (*see* Supplementary Material Table *S1*). In 2004, Sotou *et al*. first found that the β-angle of the 4O structure with $(2\bar{2})$ stacking order is 90° through selected area diffraction pattern (SADP) results in the $Ni_{50}Mn_{37.5}Sn_{12.5}$ alloy, anticipating a substantial MFIS due to lower twin stresses[1]. In 2020, Chulist and Czaja introduced a stacking sequence $(010\bar{1})$ in line with the concept of atomic shuffling[25]. Subsequently, Lin analyzed the crystallographic characteristics of the 4O martensite in the $Ni_{50}Mn_{37.5}Sn_{12.5}$ alloy using X-ray diffraction and refined the Rietveld method[26]. While extensive research has been conducted experimentally on the performance of doped alloys, the effects of Fe, Co, and Cu doping on the martensitic transformation sequence and magnetic properties including the intermediate 4O martensite, remains inadequately elucidated in the literature.

In this study, we chose the $Ni_2Mn_{1.5}Sn_{0.5}$ alloy as the parent system. This is because the

martensitic transformation can only be observed with $x \geq 0.5$ in the Mn-rich $Ni_2Mn_{1+x}Sn_{1-x}$ system. Moreover, commonly studied compositions in experiments are located close to it. Employing the first-principle calculations, three different alloying systems Ni-Mn-Sn-*Z* (*Z* = Fe, Co, and Cu) were systematically studied. For each system, first, the preferred atomic occupation of the doped *Z* atom was determined, and then the phase stability, martensitic transformation, magnetic properties, mechanical properties, and electronic structure of the Ni-Mn-Sn-*Z* alloys were systematically studied. This effort is expected to offer valuable insights for the further development of magnetic shape memory alloys.

2 Calculation details

All calculations were carried out by using the first-principles method based on density functional theory (DFT) with the Vienna ab initio Simulation Package (VASP)[27,28]. The projector augmented-wave (PAW) pseudopotential approach was employed to describe the interaction between ions and electrons. To handle the exchange-correlation potential, we opted for the Perdew–Burke–Ernzerhof (PBE) implementation of generalized gradient approximation (GGA)[29-31]. The valence electronic configurations for the Ni, Mn, Sn, Fe, Co, and Cu PAW pseudopotentials were $3d^8 4s^2$, $3d^6 4s^1$, $4d^{10} 5s^2 5p^2$, $3d^7 4s^1$, $3d^8 4s^1$, and $3d^{10} 4s^1$, respectively. First, the preferential occupation manner in the austenite was determined using a 16-atom unit cell and sampled Brillouin zone using Monkhorst–pack method with 12×12×12 *k*-points. As the experiments were carried out under low concentrations of the substituents, it is necessary to impose constraints on the value of *x* and construct a 32-atom supercell to perform calculations for the austenite, 4O and NM martensites at various doping concentrations (Ni-Mn-Sn-Z_x (x = 0, 0.125, 0.25, 0.375)). The *k*-point grids used for the austenite, 4O martensite, and NM martensite were as follows: 12×12×6, 5×13×17, and 10×10×10, respectively. The plane-wave cutoff energies of 351 eV (Ni-Mn-Sn-Fe_x/Co_x alloys) and 385 eV (Ni-Mn-Sn-Cu_x alloys) were set respectively during structural relaxation. The convergence criteria for total energy and force on individual atoms were set to be 10^{-4} eV and 0.02 eV/Å, respectively. Detailed crystallographic information on 4O martensite is available from Ref.[32]. The elastic constants C_{ij} were calculated using the strain-energy method[33].

The stability of an alloy composition can be evaluated by calculating its formation energy (E_{form}),

as shown in Eq. (2-1):

$$E_{\mathrm{form}} = \frac{E_{\mathrm{total}} - N_{\mathrm{Ni}}E_{\mathrm{Ni}} - N_{\mathrm{Mn}}E_{\mathrm{Mn}} - N_{\mathrm{Sn}}E_{\mathrm{Sn}} - N_{\mathrm{Z}}E_{\mathrm{z}}}{N_{\mathrm{total}}} \times 1000 \quad (2\text{-}1)$$

Where E_{total} represents the total ground-state energy, N_{X} (X = Ni, Mn, Sn, *Z*) signifies the number of corresponding elements X, and E_{X} denotes the ground-state energy per atom of each pure element X in its reference bulk state. The magnetic exchange parameters J_{ij} was calculated through the spin-polarized-relativistic Korringa-Kohn-Rostoker (SPR-KKR) program package[34,35]. The self-consistent field (SCF) calculations have been performed with 0.01 mRy as the energy convergence tolerance. For the real part of the lowest energy, E_{min} was set to -0.2 Ry. The SCF mixing parameter was set to 0.2, and the SCF iterations were carried out for a total of 200 steps.

3 Results and discussion

3.1 Site preferences and magnetic ground states

Experimental[36,37] and theoretical[38,39] investigations have revealed that the physical properties of alloys, such as phase stability, martensitic transformation, and magnetic properties, are strongly dependent on the atomic disorder (atomic occupation). Some research groups were interested in substituting Ni or Mn with Fe, Co, or Cu[40-45], while others focused on replacing Sn with Cu[46]. However, the available experimental data are insufficient to determine the preferred sublattice for the doped fourth element. Thus, we initially compare the E_{form} of different possible occupations to determine the favored occupation of Fe, Co, and Cu atoms in the austenite of Ni-Mn-Sn alloys. This section will examine both direct and indirect occupations. Direct occupation is defined as when the *Z* atoms directly occupy the sublattice of the replaced element, as depicted in Fig. 1(a)-(d), while all other cases fall under the category of indirect occupation, as shown in Fig.1(e)-(g) and Supplementary Material Fig. *S*1. For instance, considering the $Ni_{1.75}Mn_{1.5}Sn_{0.5}Z_{0.25}$ alloy to elucidate direct and indirect occupation. *Z*→Ni means that the *Z* atom directly occupies the Ni sublattice (Fig.1 (a)); *Z*→Mn_{Mn}→Ni means that the *Z* atom occupies the position of the normal Mn atom (Mn_{Mn}), forcing the Mn_{Mn} atom to occupy the Ni sublattice (Fig.1 (e)); and so on for other cases. Two cases were considered when substituting Mn, namely substituting Mn_{Mn} atoms and substituting the Mn atoms at the Sn sublattice (Mn_{Sn}).

Furthermore, all possible magnetic configurations were taken into account for the austenite, as shown in Fig. 1(h). In cases where the atomic occupancy does not involve Mn atoms occupying the Ni sublattice (Mn_{Ni}), only the ferromagnetic (FM) and ferrimagnetic (FIM) states need to be considered. "FM" and "FIM" respectively represent that the spin direction of the atomic magnetic moments of Mn_{Sn} is parallel or antiparallel to that of Ni, *Z*, Sn, and Mn_{Mn}. In instances involving Mn_{Ni} atoms, the ferrimagnetic state necessitates further refinement into distinct cases, such as FIM1, FIM2, and FIM3. "FIM1" represents the spin direction of the atomic magnetic moments of Mn_{Sn} and Mn_{Ni} are antiparallel to that of Mn_{Mn}. If the magnetic moment direction of Mn_{Ni} or Mn_{Sn} arranges antiparallel to that of Mn_{Mn}, they are named "FIM2" or "FIM3", respectively.

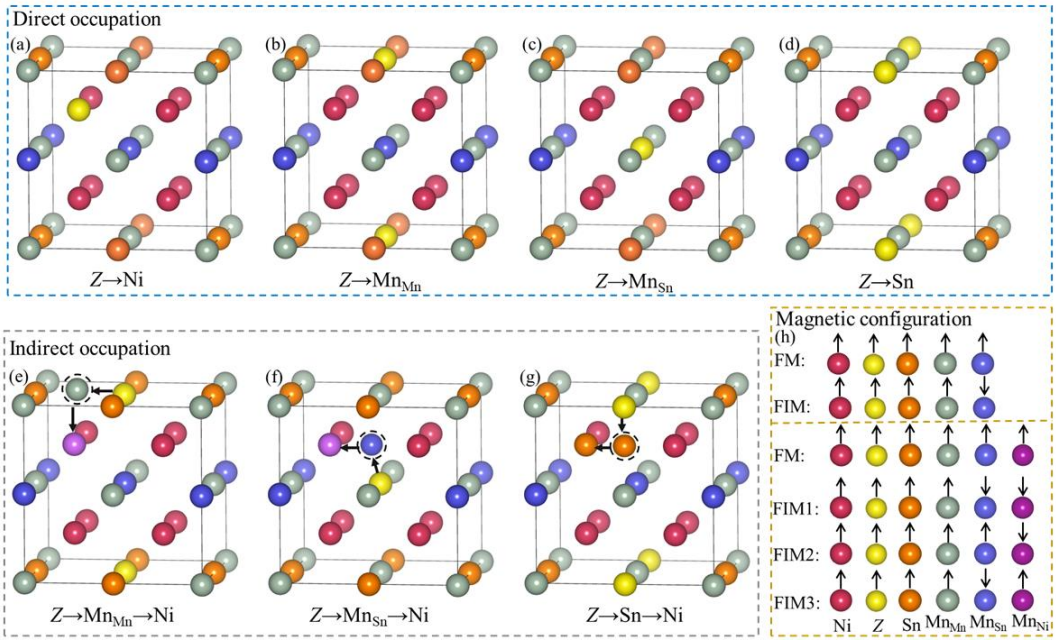

Fig. 1. Crystal structure of direct occupation for *Z* (*Z* = Fe, Co, and Cu) atoms (x = 0.25) substituted (a) $Ni_{1.75}Mn_{1.5}Sn_{0.5}Z_{0.25}$, (b) $Ni_2Mn_{Mn0.75}Mn_{Sn0.5}Sn_{0.5}Z_{0.25}$, (c) $Ni_2Mn_{Mn}Mn_{Sn0.25}Sn_{0.5}Z_{0.25}$, and (d) $Ni_2Mn_{1.5}Sn_{0.25}Z_{0.25}$ alloys, and (e)-(g) indirect occupation of $Ni_{1.75}Mn_{1.5}Sn_{0.5}Z_{0.25}$ alloy. (h) Schematic diagram of atomic spin directions in FM, FIM, FIM1, FIM2, and FIM3 states (The ↑ and ↓ represent spin direction of atomic magnetic moment).

The E_{form} of austenite for all possible magnetic states based on the occupations were taken into consideration, as depicted in Fig. 2. In the case of the Fe-doped alloys (Fig. 2(a)), the E_{form} of direct occupation is lower than that of indirect occupation when Fe atoms substitute Ni or Mn_{Mn} atoms. Whereas when Fe is introduced by substituting Mn_{Sn}, the E_{form} of the indirect occupation (Fe→Ni→Mn_{Sn}) with FM state is the lowest. When Fe atoms replace Sn atoms, the formation energy difference between the Fe→Sn occupation with FM state and the Fe→Mn_{Mn}→Sn occupation with

FIM state is only 0.7 meV/atom, suggesting that both occupation manners may coexist in the Sn-deficient alloys. Notably, the Fe atoms directly replacing the Mn_{Mn} sublattice in the FIM state exhibit the lowest E_{form}. Therefore, it is confirmed that Fe atoms preferentially directly occupy the sublattice of Mn_{Mn} in Ni-Mn-Sn alloys.

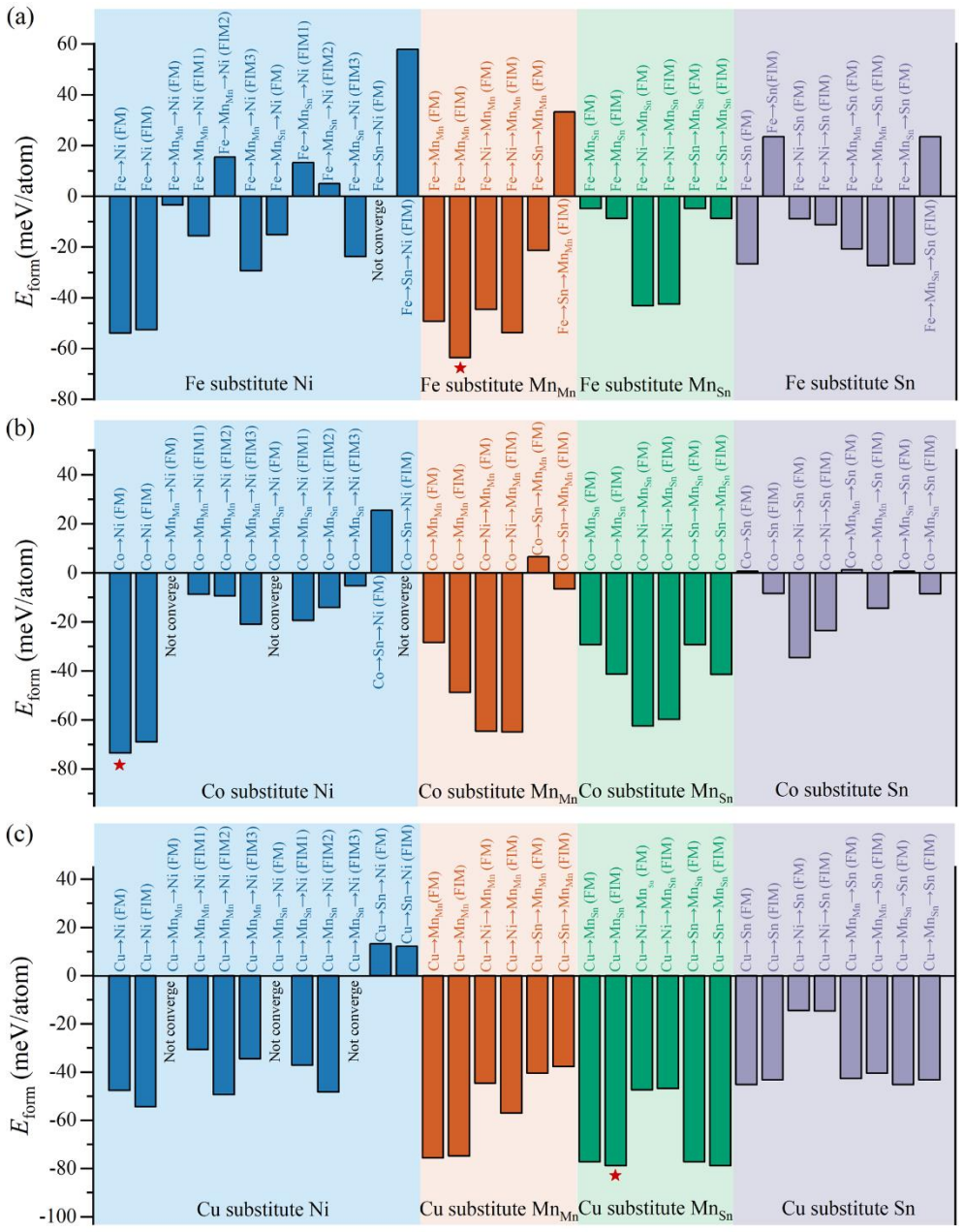

Fig. 2. E_{form} of austenite for (a) Fe, (b) Co, or (c) Cu atoms (x = 0.25) substitute Ni, Mn_{Mn}, Mn_{Sn}, or Sn sublattices in $Ni_2Mn_{1.5}Sn_{0.5}$ alloys with different occupation manners ($Ni_{1.75}Mn_{1.5}Sn_{0.5}Z_{0.25}$ (blue area), $Ni_2Mn_{Mn0.75}Mn_{Sn0.5}Z_{0.25}$ (orange area), $Ni_2Mn_{Mn}Mn_{Sn0.25}Sn_{0.5}Z_{0.25}$ (green area), and $Ni_2Mn_{1.5}Sn_{0.25}Z$ (purple area)).

As illustrated in Fig. 2(b), when Ni is substituted by Co, the lowest E_{form} occurs in the FM state when Co atoms directly occupy the Ni sublattice. For substitutions at the Mn or Sn sites, Co atoms

still preferentially occupy the Ni sublattice, which forces Ni to occupy the Mn or Sn sublattice, resulting in the lowest E_{form} for these configurations. Notably, regardless of the occupation manners, the configuration in which Co atoms directly occupy the Ni sublattice (Co→Ni) consistently exhibits the lowest E_{form}. This indicates a strong preference for Co atoms to occupy the Ni sublattice.

In the Cu-doped alloys (Fig.2 (c)), the E_{form} is lowest when the direct occupation is applied to the Ni-, Mn_{Mn}-, and Sn-deficient alloys. It is worth noting that when Cu substitutes for Mn_{Sn}, the E_{form} in the FIM state of direct occupation is the same as that of indirect occupation of Cu→Sn→Mn_{Sn} configuration, and it is the lowest E_{form} in all occupation manners for Cu-doped system. For the convenience of calculation, the Cu atoms are set to directly replace the Mn_{Sn} sublattice when calculating the physical properties of the Cu-doped alloys. In summary, it has been determined that Fe, Co, and Cu atoms tend to preferentially directly substitute Mn_{Mn}, Ni, and Mn_{Sn} sublattices in Ni-Mn-Sn alloys, respectively.

Subsequently, to determine the magnetic states of austenite, 4O and NM martensites in Fe, Co, and Cu-doped Ni-Mn-Sn alloys, the E_{form} of austenite, 4O and NM martensites in both FM and FIM states were calculated respectively, and the results are presented in Fig. 3. It was observed that the FIM state is energetically more favorable for the austenite, 4O and NM martensites in the $Ni_2Mn_{1.5}Sn_{0.5}$ alloy. In all the studied alloys, except for the 4O martensite in the $Ni_{1.625}Co_{0.375}Mn_{1.5}Sn_{0.5}$ alloy, the E_{form} of the 4O and NM martensites in the FIM state is consistently lower than that of the FM state, which means the 4O and NM martensites exist stably in the FIM state in these alloys. However, in the $Ni_{1.625}Co_{0.375}Mn_{1.5}Sn_{0.5}$ alloy, the E_{form} of the FIM state 4O martensite is only 0.88 meV lower than that of the FM state, leading to the potential coexistence of the two magnetic states.

The magnetic state of the austenite exhibits a more complex stability behavior. For the $Ni_2Mn_{1.5-x}Fe_xSn_{0.5}$ alloys (Fig. 3(a)), the E_{form} of the austenite in the FIM state is consistently lower than that in the FM state, suggesting that austenite exhibits a preference for the FIM state within the range of $x = 0 \sim 0.375$. In the case of the $Ni_{2-x}Co_xMn_{1.5}Sn_{0.5}$ alloys (Fig. 3(b)), the formation energy difference between the FM and FIM state ($\triangle E_{FM-FIM}$) of austenite is only -0.1 meV/atom at $x = 0.125$. This small $\triangle E_{FM-FIM}$ indicates that both magnetic configurations are nearly identical in energy and may coexist in the alloys. As the Co content increases, the FM state becomes more energetically favorable for the

austenite at x = 0.25 and 0.375, signifying a preference for the FM state in the austenite. In the $Ni_2Mn_{1.5-x}Cu_xSn_{0.5}$ alloys, the E_{form} of the FIM state in the austenite is consistently lower than that of the FM state up to x = 0.375 (Fig. 3(c)), indicating that austenite presents the FIM state. At x = 0.375, $\triangle E_{FM\text{-}FIM}$ is only -0.58 meV/atom, implying that the two magnetic states may coexist. In addition, the formation energies of the alloys with the most stable magnetic states are all negative, indicating that they are thermodynamically stable, and can be synthesized experimentally.

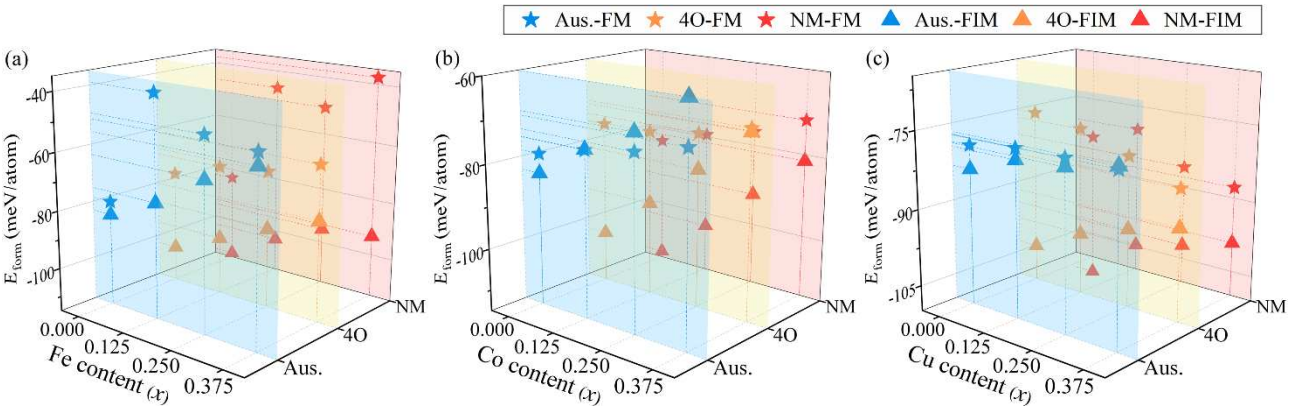

Fig. 3. Composition and possible phases dependence of E_{form} for (a) $Ni_2Mn_{1.5-x}Fe_xSn_{0.5}$, (b) $Ni_{2-x}Co_xMn_{1.5}Sn_{0.5}$, and (c) $Ni_2Mn_{1.5-x}Cu_xSn_{0.5}$ systems.

3.2 Phase stability and martensitic transformation

As shown in Fig. 4(a_1)-(c_1), the increasing E_{form} for the three phases indicates a decrease in the stability of the austenite, 4O, and NM phases with increasing Fe, Co, and Cu contents. Additionally, a clear regularity emerges between the E_{form} of each phase and the doping content x, and this relationship can be derived through fitting:

(1) For the $Ni_2Mn_{1.5-x}Fe_xSn_{0.5}$ alloys:

$$E_{form\text{-}Aus.}=75.14x-83.51 \quad (3\text{-}1)$$

$$E_{form\text{-}4O}=60.41x-102.66 \quad (3\text{-}2)$$

$$E_{form\text{-}NM}=-133.76x^2+105.30x-113.67 \quad (3\text{-}3)$$

(2) For the $Ni_{2-x}Co_xMn_{1.5}Sn_{0.5}$ alloys:

$$E_{form\text{-}Aus.}=-72.32x^2+59.34x-82.83 \quad (3\text{-}4)$$

$$E_{form\text{-}4O.}=85.10x-102.97 \quad (3\text{-}5)$$

$$E_{form\text{-}NM}=85.40x-113.66 \quad (3\text{-}6)$$

(3) For the $Ni_2Mn_{1.5-x}Cu_xSn_{0.5}$ alloys:

$$E_{\text{form-Aus.}}=-33.76x^2+27.50x-82.99 \quad (3\text{-}7)$$

$$E_{\text{form-4O.}}=29.28x-102.21 \quad (3\text{-}8)$$

$$E_{\text{form-NM}}=-91.84x^2+70.76x-113.10 \quad (3\text{-}9)$$

where $E_{\text{form-Aus.}}$, $E_{\text{form-4O}}$, and $E_{\text{form-NM.}}$ represent the E_{form} of austenite, 4O and NM martensites, respectively, and x represents the doping content in each system. These relationship equations provide a concise and rigorous representation of the observed trends, facilitating convenient prediction of E_{form} for various phases in Ni-Mn-Sn-Z_x (Z = Fe, Co, and Cu) systems with different compositions. This approach enables the estimation of phase stability and offers preliminary insights into the possibility of martensitic transformations. By doing so, it circumvents the need for laborious experimental procedures, offering a more efficient approach to alloy composition design.

To evaluate the driving force of the martensitic transformation, we calculated the formation energy differences between austenite and 4O ($\triangle E_{\text{Aus.-4O}}$) /NM ($\triangle E_{\text{Aus.-NM}}$) martensite, as well as between 4O and NM ($\triangle E_{\text{4O-NM}}$) martensites, as shown in Fig. 4(a_2)-(c_2). In the case of the $Ni_2Mn_{1.5-x}Fe_xSn_{0.5}$ (Fig. 4(a_2)) and $Ni_2Mn_{1.5-x}Cu_xSn_{0.5}$ (Fig. 4(c_2)) alloys, the values of $\triangle E_{\text{Aus.-4O}}$ and $\triangle E_{\text{4O-NM}}$ are both larger than 0 meV/atom, indicating that these alloys have great thermodynamic possibility to undergo two-step martensitic transformations. Therefore, the possible martensitic transformation sequences are as follows: $\text{Aus.}^{\text{FIM}}\rightarrow 4\text{O}^{\text{FIM}}\rightarrow \text{NM}^{\text{FIM}}$ ($0 \le x \le 0.375$) for the $Ni_2Mn_{1.5-x}Fe_xSn_{0.5}$ alloys, $\text{Aus.}^{\text{FIM}}\rightarrow 4\text{O}^{\text{FIM}}\rightarrow \text{NM}^{\text{FIM}}$ ($0 \le x < 0.375$) and $\text{Aus.}^{\text{FM/FIM}}\rightarrow 4\text{O}^{\text{FIM}}\rightarrow \text{NM}^{\text{FIM}}$ ($x = 0.375$) for the $Ni_2Mn_{1.5-x}Cu_xSn_{0.5}$ alloys. Furthermore, a larger formation energy difference means a greater phase transformation driving force and a correspondingly higher martensitic transformation temperature (T_M). As Fe content increases, the $\triangle E_{\text{Aus.-4O}}$ and $\triangle E_{\text{Aus.-NM}}$ generally exhibit an increasing trend. In contrast, with increasing Cu content, the trend is reversed. Hence, it can be deduced that the T_M increases gradually with increasing Fe content in the $Ni_2Mn_{1.5-x}Fe_xSn_{0.5}$ alloys, while it decreases with increasing Cu content in the $Ni_2Mn_{1.5-x}Cu_xSn_{0.5}$ alloys. These trends are highly consistent with the experimental results[47,48].

In the $Ni_{2-x}Co_xMn_{1.5}Sn_{0.5}$ alloy (Fig. 4(b_2)), the $\triangle E_{\text{Aus.-NM}}$ is considerably higher than $\triangle E_{\text{4O-NM}}$ before reaching x = 0.375, suggesting a stronger driving force for the martensitic transformation compared to the intermediate martensitic transformation. However, at x = 0.375, the $\triangle E_{\text{Aus.-NM}}$ gradually approaches $\triangle E_{\text{4O-NM}}$, with the $\triangle E_{\text{Aus.-4O}}$ is only 0.55 meV/atom, indicating a low possibility

of austenite transforming into 4O martensite. Hence, the potential martensitic transformation sequence in the $Ni_{2-x}Co_xMn_{1.5}Sn_{0.5}$ alloy during the cooling process can be summarized as follows: Aus.^{FIM}→4O^{FIM}→NM^{FIM} ($0 \leq x < 0.125$), Aus.$^{FIM/FM}$→4O^{FIM}→NM^{FIM} ($x = 0.125$), Aus.^{FM}→4O^{FIM}→NM^{FIM} ($0.125 < x < 0.375$), and Aus.^{FM}→NM^{FIM} ($x = 0.375$). With the increase in Co content, both the $\triangle E_{Aus.\text{-}NM}$ and $\triangle E_{Aus.\text{-}4O}$ decrease. This indicates a weakening of the driving force for martensitic transformation, resulting in a lower T_M, which is consistent with experimental observations[49]. It is important to emphasize that when analyzing the physical properties of alloys in subsequent calculations, in cases where two magnetic states coexist, we choose to examine the state with the relatively lower E_{form}.

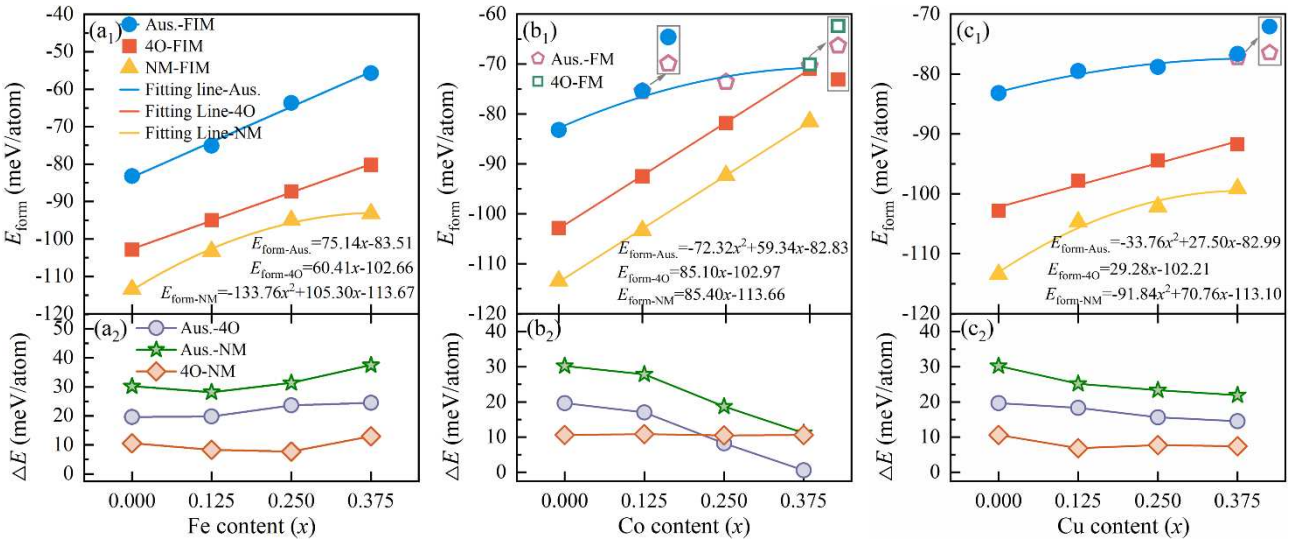

Fig. 4. Composition dependence of E_{form} and ΔE for (a_1)-(a_2) $Ni_2Mn_{1.5-x}Fe_xSn_{0.5}$, ($b_1$)-($b_2$) $Ni_{2-x}Co_xMn_{1.5}Sn_{0.5}$, and ($c_1$)-($c_2$) $Ni_2Mn_{1.5-x}Cu_xSn_{0.5}$ systems. The lines in the top figure represent linear fit to data points.

3.3 Mechanical properties

Mechanical performance stands as a fundamental property of materials and plays a crucial role in the case of Ni-Mn-based Heusler alloys. Table 1 presents the elastic constants of austenite, 4O and NM martensites for the $Ni_2Mn_{1.5}Sn_{0.5}$, $Ni_2MnFe_{0.5}Sn_{0.5}$, $Ni_{1.5}Co_{0.5}Mn_{1.5}Sn_{0.5}$, and $Ni_2MnCu_{0.5}Sn_{0.5}$ alloys. Due to the necessity of employing standard unit cell structures for the calculation of elastic constant, we selected the aforementioned four alloys to represent the matrix and different alloying systems, allowing for a qualitative analysis of the impact of alloying with 3*d*-transition elements (Z = Fe, Co, and Cu) on mechanical behavior. The elastic stability criteria are as follows: for the cubic austenite, $C_{11} - C_{12} > 0$, $C_{11} + 2C_{12} > 0$, $C_{44} > 0$; for the orthorhombic 4O martensite, $C_{11} > 0$, $C_{11}C_{22} >$

C_{12}^2, $C_{11}C_{22}C_{33} + 2C_{12}C_{13}C_{23} - C_{11}C_{23}^2 - C_{22}C_{13}^2 - C_{33}C_{12}^2 > 0$, $C_{44} > 0$, $C_{55} > 0$, $C_{66} > 0$; for the tetragonal NM martensite, $C_{11} > |C_{12}|$, $2C_{13}^2 < C_{33}(C_{11} + C_{12})$, $C_{44} > 0$, $C_{66} > 0$[50]. According to the criteria, the 4O and NM martensites exhibit mechanical stability across the four alloys, but for the austenite, only the $Ni_{1.5}Co_{0.5}Mn_{1.5}Sn_{0.5}$ alloy is mechanically stable. The austenite of the other three alloys does not meet the condition $C_{11} - C_{12} > 0$, which indicates that austenite is unstable and prone to structural transformation[51,52]. For the $Ni_{1.5}Co_{0.5}Mn_{1.5}Sn_{0.5}$ alloy, according to equations (3-4) and (3-6), the formation energies of austenite, 4O and NM martensite phases are -71.24, -60.42, and -70.96 meV/atom, respectively. The driving force for transformation ($\triangle E_{Aus.-NM}$ = 0.28 meV/atom) is notably small, suggesting a high probability that martensitic transformation will not occur. Furthermore, relevant mechanical performance parameters can be computed by formulas from the literature[53]. The shear modulus G is calculated as the mean of shear moduli given by formalisms of Voigt (G_V) and Reuss (G_R). Since the experimental G value is close to the calculated G_V value in many Ni-Mn-based Heusler alloys, we approximated G as G_V[51,54].

Based on the data from Table 1, the G_V and Young's modulus (E) of the austenite in all four alloys are both lower than those of the 4O and NM martensites, indicating that martensites have greater stiffness than austenite in the same composition[55]. Furthermore, the austenites have higher Cauchy pressure (C^p) and Pugh's ratio (B/G_V) (the ratio of bulk modulus B to G_V) values than the 4O and NM martensites. The B/G_V ratio serves as an indicator of brittleness or ductility for a material, where $B/G_V > 1.75$ is associated with ductility[56]. Generally, higher B/G_V values correspond to improved toughness, and a positive C^p value implies the presence of strong metallic bonds and excellent toughness in the material[57]. The effectiveness of these two parameters has been validated in Ni-Mn-based Heusler alloys. Currently, they are widely utilized for assessing the mechanical properties of Ni-Mn-based Heusler alloys[52,58]. Therefore, the austenites exhibit higher plastic toughness compared to the 4O and NM martensites in the matrix and different alloying systems. The subsequent discussion on the elastic modulus of different alloys will specifically address the austenite.

Table 1 Elastic constants of $Ni_2Mn_{1.5}Sn_{0.5}$, $Ni_2MnFe_{0.5}Sn_{0.5}$, $Ni_{1.5}Co_{0.5}Mn_{1.5}Sn_{0.5}$, and $Ni_2MnCu_{0.5}Sn_{0.5}$ alloys.

Elastic constants	$Ni_2Mn_{1.5}Sn_{0.5}$			$Ni_2MnFe_{0.5}Sn_{0.5}$			$Ni_{1.5}Co_{0.5}Mn_{1.5}Sn_{0.5}$			$Ni_2MnCu_{0.5}Sn_{0.5}$		
	Aus.	4O	NM	Aus.	4O	NM	Aus.	4O	NM	Aus.	4O	NM
C_{11}/GPa	137.55	254.94	189.11	135.91	269.26	204.21	173.12	247.37	250.59	110.97	269.46	215.05
C_{12}/GPa	145.46	82.74	89.95	152.04	86.61	104.48	139.03	135.24	51.06	169.00	95.30	83.75
C_{13}/GPa	–	84.73	136.46	–	93.24	133.22	–	60.75	141.49	–	86.87	140.76
C_{22}/GPa	–	201.07	–	–	208.48	–	–	173.49	–	–	211.61	–
C_{23}/GPa	–	119.09	–	–	114.77	–	–	135.90	–	–	132.96	–
C_{33}/GPa	–	241.47	192.63	–	257.70	211.38	–	250.92	185.76	–	242.67	175.61
C_{44}/GPa	99.42	68.22	95.34	97.98	63.75	95.15	101.08	98.91	99.79	101.25	76.18	98.32
C_{55}/GPa	–	38.84	–	–	46.42	–	–	29.67	–	–	32.88	–
C_{66}/GPa	–	68.166	81.61	–	59.80	83.25	–	99.32	31.21	–	76.07	65.11
B/GPa	142.82	141.18	144.06	146.66	147.18	151.30	150.39	148.40	150.56	149.66	150.44	148.47
G_v/GPa	58.07	62.44	68.32	55.56	63.38	71.30	67.47	68.24	69.68	49.15	64.26	68.38
v	0.32	0.31	0.30	0.33	0.31	0.30	0.30	0.30	0.30	0.35	0.31	0.30
B/G_v	2.46	2.26	2.11	2.64	2.32	2.12	2.23	2.17	2.16	3.04	2.34	2.17
C^p/GPa	46.04	14.52	-5.39	54.06	22.86	9.33	37.95	36.34	-48.74	67.75	19.12	-14.57
E/GPa	153.42	163.25	176.99	147.99	166.28	184.87	176.07	177.51	181.11	132.89	168.76	177.84

The austenites of $Ni_2MnFe_{0.5}Sn_{0.5}$ and $Ni_2MnCu_{0.5}Sn_{0.5}$ alloys exhibit higher Poisson's ratio (v), Pugh's ratio, and C^p compared to the $Ni_2Mn_{1.5}Sn_{0.5}$ ternary alloy. The v also can describe the lattice stability and plasticity of the alloy[59]. Generally, when v is greater than 0.33, it means that the ductility of a metallic material is good, and a higher v value indicates better plasticity[60]. Therefore, the plasticity and toughness are significantly enhanced after Fe or Cu doping. These calculated results provide a robust explanation for the experimental findings in the existing literature, such as the $Ni_{50}Mn_{37-x}Fe_xSn_{13}$ (x = 10) (corresponding to the calculated composition $Ni_2Mn_{1.48-x}Fe_xSn_{0.52}$ (x = 0.4)) alloy achieving a strength of ~1533 MPa and a ductility of ~17.7%[61].

Moreover, the austenites of $Ni_{1.5}Co_{0.5}Mn_{1.5}Sn_{0.5}$ alloy exhibit the lowest v, Pugh's ratio, and C^p but the highest G_v and E compared to the other alloys. This suggests that from a theoretical standpoint, Co-doping may reduce the alloy's toughness but enhance its stiffness. To further validate the accuracy of the mechanical performance calculations, compression tests were conducted on $Ni_2Mn_{1.5-x}Fe_xSn_{0.5}$, $Ni_{2-x}Co_xMn_{1.5}Sn_{0.5}$, and $Ni_2Mn_{1.5-x}Cu_xSn_{0.5}$ (x = 0~0.375). The results of these tests align with the predictions presented in this section, confirming the reliability of our computational outcomes (*see* experimental evidence in Supplementary Material Section S3).

The elastic anisotropy plays a pivotal role in influencing the microcrack behavior and

mechanical durability of materials. As elastic anisotropy is inherently associated with crystallographic direction, the three-dimensional surface construction stands out as the optimal means to directly characterize elastic anisotropy. Consequently, Fig. 5 and Fig. 6 present the spatial dependence of Young's modulus for the austenite, 4O and NM martensites in the four alloys. Notably, due to the mechanical instability exhibited by the austenite in the $Ni_2Mn_{1.5}Sn_{0.5}$, $Ni_2MnFe_{0.5}Sn_{0.5}$, and $Ni_2MnCu_{0.5}Sn_{0.5}$ alloys, rendering them unsuitable for representation in a three-dimensional (3D) Young's modulus graph. Therefore, the austenites of these four alloys are individually depicted in polar coordinate form for a comprehensive discussion, as shown in Fig. 5 (*see* 3D Young's modulus for the austenite of the $Ni_{1.5}Co_{0.5}Mn_{1.5}Sn_{0.5}$ alloy in Supplementary Material Fig. *S*3).

According to Fig. 5, for the austenite in the $Ni_2Mn_{1.5}Sn_{0.5}$, $Ni_2MnFe_{0.5}Sn_{0.5}$, and $Ni_{1.5}Co_{0.5}Mn_{1.5}Sn_{0.5}$, alloys, the maximum E values occur in the <111> direction, while for the $Ni_2MnCu_{0.5}Sn_{0.5}$ it occurs along the <101> direction. Notably, the minimum E values for the austenite in the four alloys are observed in the <100> direction, implying that the alloys are more prone to deformation along this direction. As shown in Fig. 6, the 4O martensites in four alloys exhibit the minimum E values along the diagonal direction in the x-z plane. Except for the $Ni_{1.5}Co_{0.5}Mn_{1.5}Sn_{0.5}$ alloy, the maximum values of the other three alloys are along the x-axis direction. The 4O martensite in the $Ni_{1.5}Co_{0.5}Mn_{1.5}Sn_{0.5}$ alloy demonstrates the maximum E value along the directions of the diagonal direction in the x-y and y-z planes. The NM martensites in the $Ni_2Mn_{1.5}Sn_{0.5}$ and $Ni_2MnFe_{0.5}Sn_{0.5}$ alloys exhibit the maximum E values along the <111> direction, while the minimum value occurs along the <100> direction. However, the NM martensite in $Ni_{1.5}Co_{0.5}Mn_{1.5}Sn_{0.5}$ alloy demonstrates the maximum E value along the diagonal direction formed by the z-axis and the x or y-axis plane, and the minimum E along the directions of the z-axis and the diagonal direction in the x-y plane. The E value of the NM martensite of the $Ni_2MnCu_{0.5}Sn_{0.5}$ alloy increases uniformly to both sides along the z-axis.

Furthermore, Fig. 6 illustrates that the anisotropy of 4O martensite decreases with Fe doping and increases with Co or Cu doping, while the anisotropy of NM martensite decreases with Fe or Cu doping and increases with Co doping. In the $Ni_2MnFe_{0.5}Sn_{0.5}$ alloy, the E differentials between the maximum and minimum values for the 4O and NM martensites are 86.56 and 131.72 MPa, respectively. These differentials are lower than those in the $Ni_2Mn_{1.5}Sn_{0.5}$ alloy (98.07 and 166.25

MPa). Additionally, the $Ni_{1.5}Co_{0.5}Mn_{1.5}Sn_{0.5}$ alloy exhibits higher *E* differentials for the 4O and NM phases compared to the $Ni_2Mn_{1.5}Sn_{0.5}$ alloy, with values of 185.25 Mpa and 192.19 Mpa, respectively. The $Ni_2MnCu_{0.5}Sn_{0.5}$ alloy exhibits a higher *E* differential for the 4O martensite compared to the $Ni_2Mn_{1.5}Sn_{0.5}$ alloy, with a value of 121.98 Mpa. Despite the anisotropy of NM martensite decreases with Cu doping, the difference in *E* becomes larger. Systematic study of the elastic anisotropy in various alloy systems will help to deeply understand the stiffness characteristics of materials across various directions under different states, and provide key reference for material selection and design.

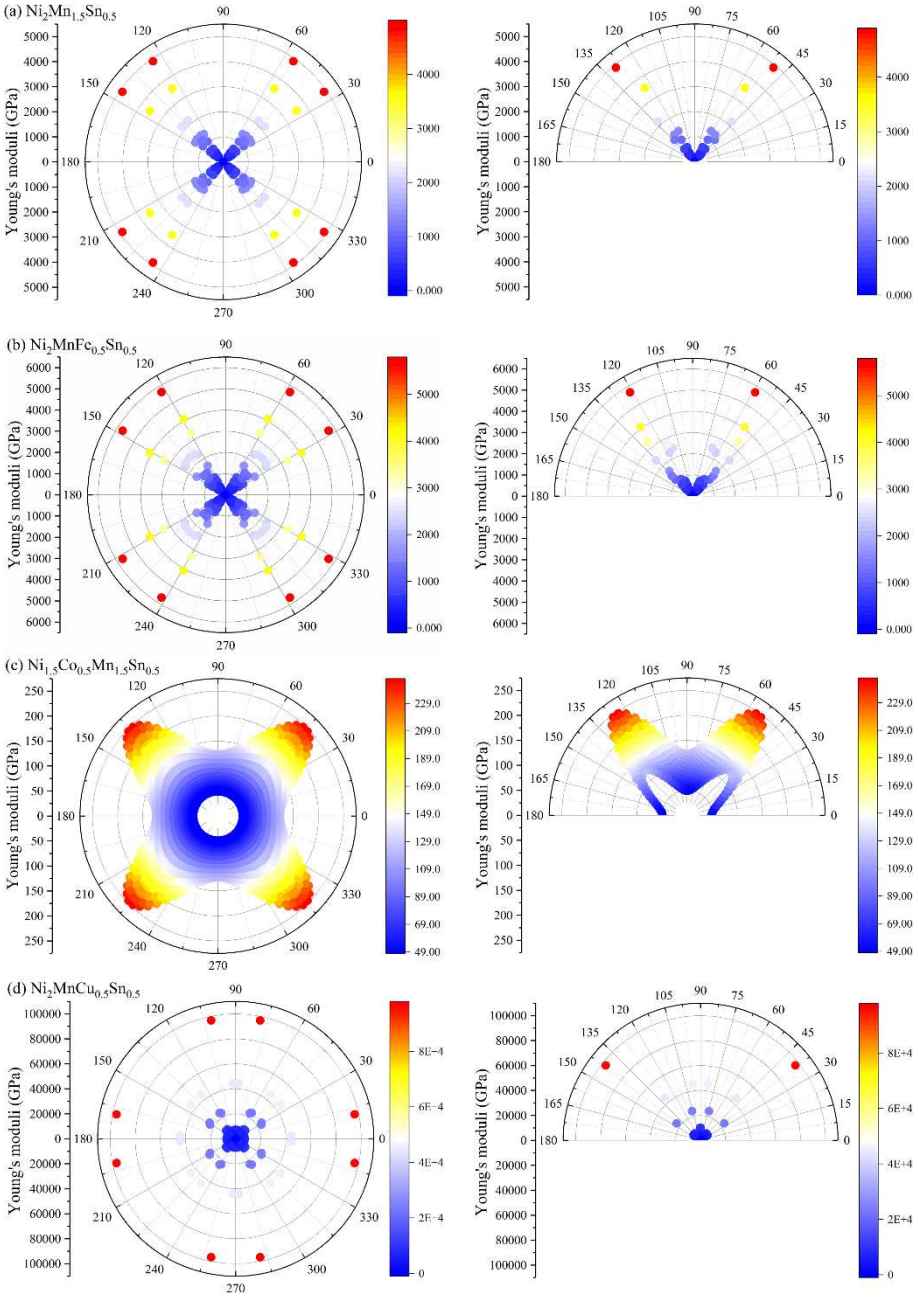

Fig. 5. Spatial dependence of single-crystal Young's modulus for austenite in (a) $Ni_2Mn_{1.5}Sn_{0.5}$, (b) $Ni_2MnFe_{0.5}Sn_{0.5}$, (c) $Ni_{1.5}Co_{0.5}Mn_{1.5}Sn_{0.5}$, and (d) $Ni_2MnCu_{0.5}Sn_{0.5}$ alloys (left column is based on phi, right column is based on theta).

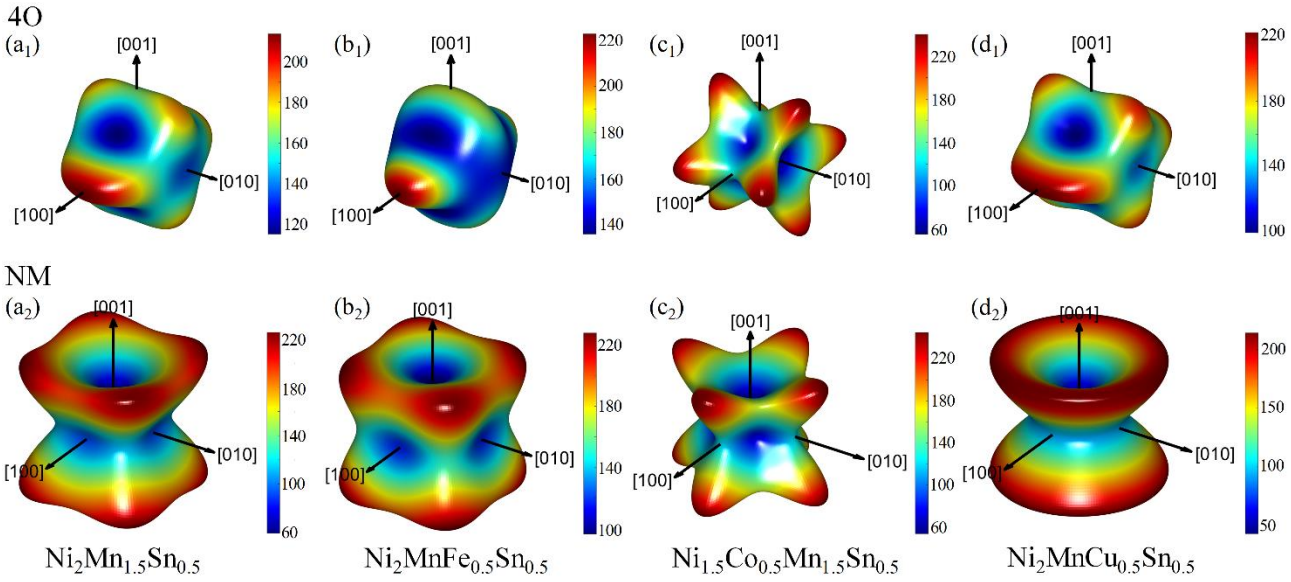

Fig. 6. Three-dimensional single-crystal Young's moduli for (a_1)-(d_1) 4O and (a_2)-(d_4) NM martensites of (a_1)-(a_2) $Ni_2Mn_{1.5}Sn_{0.5}$, (b_1)-(b_2) $Ni_2MnFe_{0.5}Sn_{0.5}$, (c_1)-(c_2) $Ni_{1.5}Co_{0.5}Mn_{1.5}Sn_{0.5}$, and ($d_1$)-($d_2$) $Ni_2MnCu_{0.5}Sn_{0.5}$ alloys.

3.4 Magnetic properties and structural parameters

Fig. 7 shows the total magnetic moments and magnetization differences of the Ni-Mn-Sn-*Z* (*Z* = Fe, Co, and Cu) alloys. Furthermore, to further delve into the underlying causes of the variation in the total magnetic moments of different phases with compositions in various alloys, we calculated the atomic magnetic moments of Ni, Mn, and Z atoms in the austenite, 4O and NM martensites, as illustrated in Fig. 8. As magnetic moments of various atoms are not fixed values, the "I" type symbols are employed to signify the range of the atomic magnetic moment, and the dots indicate the average values of magnetic moments for each atom type, to clearly show the change of atomic magnetic moment with the composition change. The atomic magnetic moment of Sn (-0.084~-0.045 μ_B) contributed insignificantly to the total magnetic moment.

From Fig. 7(a), a slight decrease in the total magnetic moment of both austenite and martensites is evident with the increasing Fe content x in the $Ni_2Mn_{1.5-x}Fe_xSn_{0.5}$ alloys. This decrease can be attributed to the lower atomic moment of Fe (2.586~2.888 μ_B) compared to the substituted Mn_{Mn} (3.160~3.629 μ_B). Notably, in the austenite of the Fe-doped alloys, the nearest neighboring distance of Mn-Mn is consistently smaller than that in the undoped alloy (2.964 Å). The nearest neighbor Mn-Mn spacing in both 4O and NM martensites is also lower than 2.964 Å, resulting in no significant change in the Mn moment (as shown in Fig. 8(a_2)). The $\triangle M_{Aus.-4O}$ (the magnetization difference

between austenite and 4O martensite) and $\triangle M_{\text{Aus.-NM}}$ (the magnetization difference between austenite and NM martensite) do not exhibit significant changes with increasing Fe content and remain close to 0 μ_B/f.u.

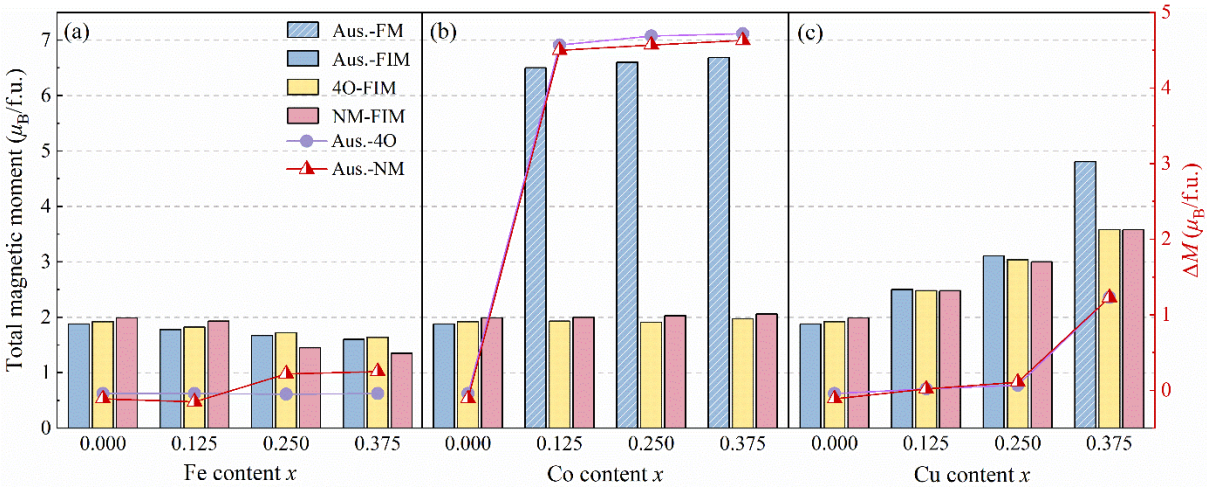

Fig. 7. Total magnetic moment per formula unit of austenite, 4O and NM martensites as well as $\triangle M$ of Aus.-4O and Aus.-NM for (a) $Ni_2Mn_{1.5-x}Fe_xSn_{0.5}$, (b) $Ni_{2-x}Co_xMn_{1.5}Sn_{0.5}$, and (c) $Ni_2Mn_{1.5-x}Cu_xSn_{0.5}$ alloys.

In the case of the $Ni_{2-x}Co_xMn_{1.5}Sn_{0.5}$ alloys (Fig. 7(b)), a magnetic moment change occurs in the austenite at x = 0.125. This shift is attributed to the substitution of Co for Ni, leading to a transition in Mn_{Mn}-Mn_{Sn} interactions from antiferromagnetic to ferromagnetic. As the Co content further increases, the magnetic moment of the austenite gradually rises, attributed to the higher atomic magnetic moment of Co compared to Ni, as shown in Fig. 8(b_1) and (b_3). However, the 4O and NM martensites remain relatively constant as x increases. Consequently, the $\triangle M_{\text{Aus.-4O}}$ and $\triangle M_{\text{Aus.-NM}}$, which were close to 0 μ_B/f.u. in the undoped alloy, undergo a transition to 4.57 μ_B/f.u. and 4.50 μ_B/f.u. at x = 0.125, gradually increasing with higher x. It is well known that higher $\triangle M$ is conducive to a more pronounced magnetocaloric response. Therefore, precise control of Co doping content in the $Ni_{2-x}Co_xMn_{1.5}Sn_{0.5}$ alloys can result in a significant MCE.

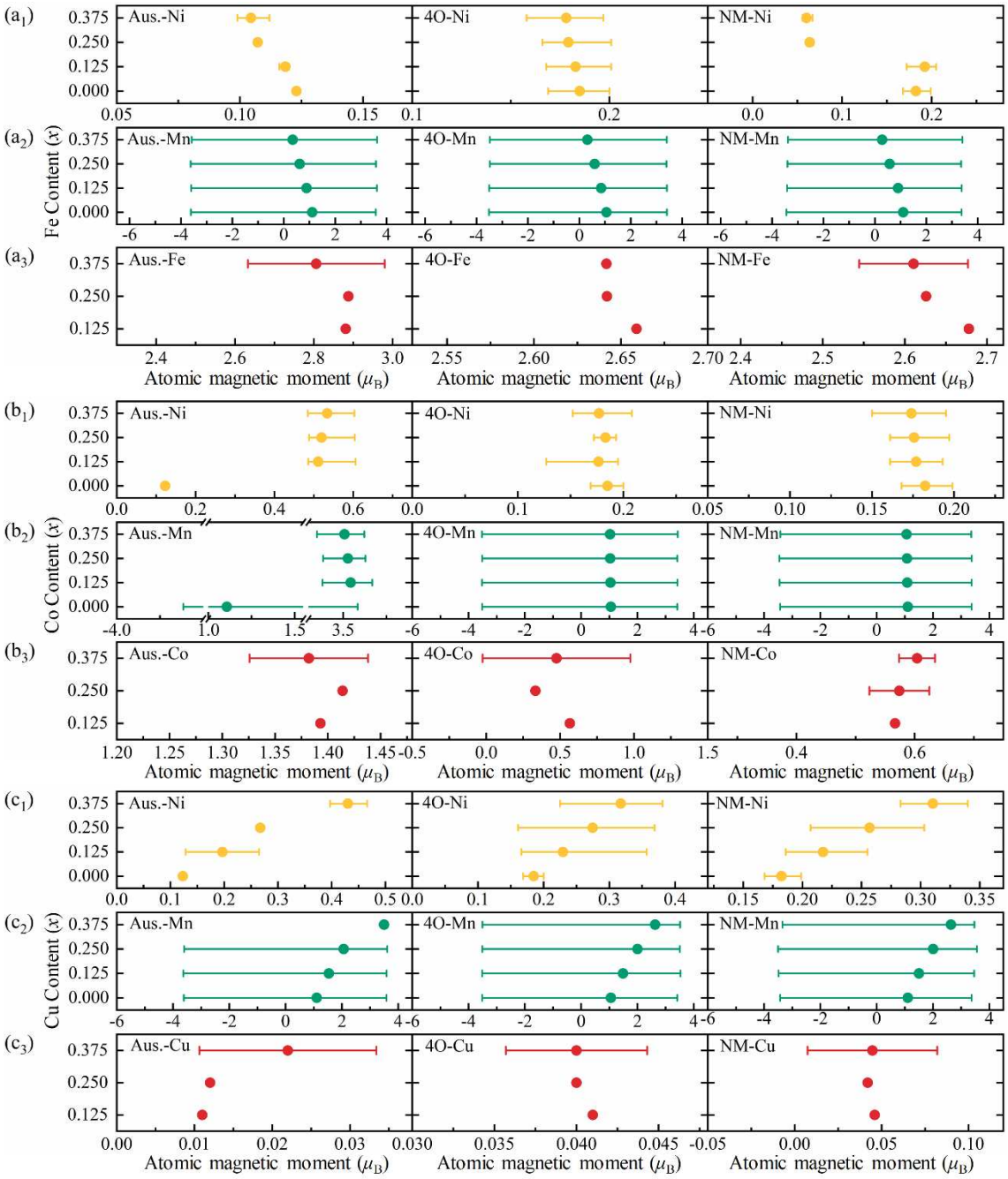

Fig. 8. Atomic magnetic moments of Aus., 4O and NM martensites for (a_1)-(a_3) $Ni_2Mn_{1.5-x}Fe_xSn_{0.5}$, ($b_1$)-($b_3$) $Ni_{2-x}Co_xMn_{1.5}Sn_{0.5}$, and ($c_1$)-($c_3$) $Ni_2Mn_{1.5-x}Cu_xSn_{0.5}$ alloys.

Concerning the $Ni_2Mn_{1.5-x}Cu_xSn_{0.5}$ alloys (Fig. 7(c)), an increase in Cu content leads to a significant rise in the total magnetic moment of both austenite and martensite. The Mn moment also increases substantially, as shown in Fig. 8(c_2). This is because Cu replaces the Mn_{Sn} sublattice, reducing the negative contribution of Mn_{Sn} atoms to the total magnetic moment. Notably, there is a remarkable enhancement of the magnetic moment in the austenite at $x = 0.375$, making the austenite

more stable in the ferromagnetic state with a magnetic moment of 4.81 μ_B/f.u. Furthermore, it can be observed from Fig. 8(c_2) that when x = 0.375, all the Mn moments in the austenite are positive, indicating ferromagnetic coupling among all the Mn atoms. Consequently, the magnetization differences between the austenite and martensites increase. From the dotted line graph in Fig. 7(c), for $x \leq 0.25$, both the $\triangle M_{\text{Aus.-4O}}$ and $\triangle M_{\text{Aus.-NM}}$ show negligible changes and remain close to 0 μ_B/f.u. However, both the $\triangle M_{\text{Aus.-4O}}$ and $\triangle M_{\text{Aus.-NM}}$ increase to 1.23 μ_B/f.u. at x = 0.375. It can be inferred that with a further increase in Cu content (x > 0.375), the proportion of Mn_{Sn} will decrease correspondingly, thereby reducing the positive contribution of Mn_{Sn} atoms to the total magnetic moment of the austenite. As a result, it is highly probable that $\triangle M_{\text{Aus.-4O}}$ and $\triangle M_{\text{Aus.-NM}}$ will also decrease.

By combining the information from Fig. 7 and Fig. 8, it can be observed that the Mn atomic magnetic moments are the major contributor to the total magnetic moment of austenite, 4O and NM martensites. Additionally, the variation trend of the total magnetic moment in the FIM austenite, 4O and NM martensites corresponds to that of Mn moments. For the FM state of the austenite, the trend in total magnetic moment with composition is opposite to that of Mn atomic magnetic moments. Nevertheless, whether in the FIM or FM state of the austenite, the variation trend of the total magnetic moment aligns with that of the Ni moments.

To further explore the notable differences in the magnetic properties of the austenite due to different doping atoms, we conducted calculations by using SPR-KKR to determine the magnetic exchange parameters (J_{ij}) among atoms in the $Ni_2Mn_{1.5}Sn_{0.5}$, $Ni_2Mn_{1.25}Fe_{0.25}Sn_{0.5}$, $Ni_{1.75}Co_{0.25}Mn_{1.5}Sn_{0.5}$, and $Ni_2Mn_{1.25}Cu_{0.25}Sn_{0.5}$ alloys, as presented in Fig. 9. Comparing the J_{ij} of the Fe- and Co-doped system (Fig. 9(b) and (c)) with the undoped system (Fig. 9(a)), it was found that the ferromagnetic interaction between Ni-Mn_{Mn} and Ni-Mn_{Sn} remains unchanged. As depicted in Fig. 9(b), When Mn_{Mn} is replaced by Fe, the ferromagnetic interaction in Ni-Fe is weaker than that in Ni-Mn_{Mn}. Moreover, the antiferromagnetic interaction in Mn_{Mn}-Mn_{Sn} significantly increases compared to the undoped state. In contrast, the antiferromagnetic interaction in Mn_{Sn}-Fe is slightly stronger than the ferromagnetic interaction in Mn_{Mn}-Fe. Consequently, the substitution of Mn_{Mn} with Fe results in a reduction of the total magnetic moment.

Upon the substitution of Co for Ni, as shown in Fig. 9(c), the Mn-Co ferromagnetic interaction

is nearly twice as strong as the Ni-Mn ferromagnetic interaction. This results in a substantial improvement in the magnetic moment of the austenite in the $Ni_{1.75}Co_{0.25}Mn_{1.5}Sn_{0.5}$ alloy compared to the undoped alloy. Referring to Fig. 9(d), the substitution of Cu for Mn_{Sn} results in a slight reduction in both the ferromagnetic interactions between Ni-Mn and the antiferromagnetic interaction between Mn_{Mn}-Mn_{Sn}. However, the enhanced ferromagnetic interaction among Mn_{Mn}-Mn_{Mn} emerges as a probable contributing factor to the observed augmentation in the total magnetic moment of the austenite.

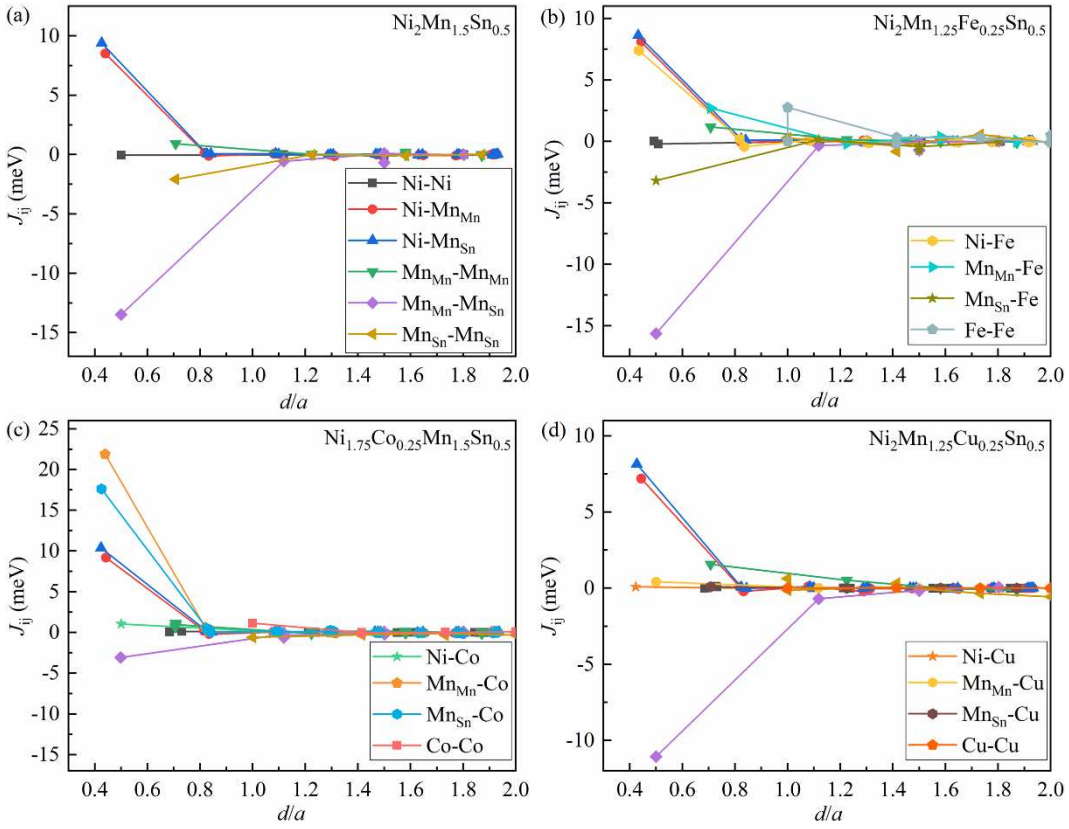

Fig. 9. Interatomic magnetic exchange parameters (J_{ij}) of austenite in (a) $Ni_2Mn_{1.5}Sn_{0.5}$, (b) $Ni_2Mn_{1.25}Fe_{0.25}Sn_{0.5}$, (c) $Ni_{1.75}Co_{0.25}Mn_{1.5}Sn_{0.5}$, and (d) $Ni_2Mn_{1.25}Cu_{0.25}Sn_{0.5}$ alloys.

Fig. 10 presents the equilibrium lattice constants and the unit cell volume of austenite, 4O and NM martensites in their most stable configurations in the Ni-Mn-Sn-*Zx* ($x = 0$~0.375) alloys. Previous studies[62,63] have reported that the main factors affecting the lattice constants are atomic radius, magnetism, and interatomic bonding. As shown in Fig. 10(a_1), when Fe replaces Mn, the smaller atomic radius of Fe (1.27 Å) compared to Mn (1.32 Å) primarily contributes to the decrease in lattice constant *a*. In the case of the 4O martensite (Fig. 10(a_2)), with the increase of Fe doping content, *a* gradually increases, *b* decreases, and *c* remains relatively unchanged. For the NM martensite (Fig.

10(a_3)), both *a* and *c* exhibit minor fluctuations within a small range.

For the austenite of the $Ni_{2-x}Co_xMn_{1.5}Sn_{0.5}$ alloys (Fig. 10(b_1)), the lattice constant *a* at $x = 0.125$ is larger than that $x = 0$. This is due to the slightly larger radius of Co atoms (1.25 Å) compared to Ni atoms (1.24 Å), and is consistent with the reported observations in the literature that alloys exhibit larger lattice constants in the ferromagnetic state compared to the non-magnetic state[64]. As the Co doping content continues to increase, the lattice constant *a* of the austenite gradually decreases. This change is primarily driven by the stronger bonding between Co atoms with larger magnetic moments and the surrounding atoms, where magnetic factors play a dominant role. For the 4O martensite (Fig. 10(b_2)), as the Co content increases, *a* and *c* gradually decrease while *b* increases. For the NM martensite (Fig. 10(b_3)), with the increase of Co content, *a* gradually increases while *c* decreases, leading to a decrease in the tetragonal distortion ($|c/a-1|$) of the martensite. Consequently, it also can be predicted that the T_M of the $Ni_{2-x}Co_xMn_{1.5}Sn_{0.5}$ alloys will decrease gradually with increasing Co content, this is consistent with the conclusion drawn from the thermodynamic $\triangle E$.

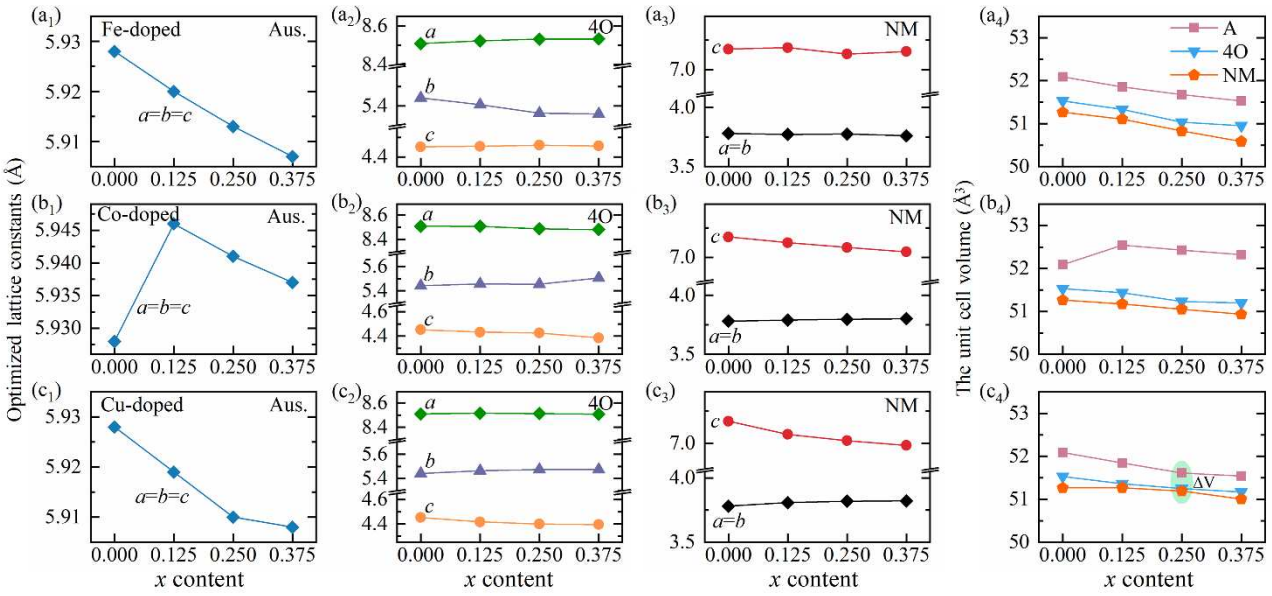

Fig. 10. Lattice constants and unit cell volume of each phase for (a_1-a_4) $Ni_2Mn_{1.5-x}Fe_xSn_{0.5}$, ($b_1$)-($b_4$) $Ni_{2-x}Co_xMn_{1.5}Sn_{0.5}$, and ($c_1$)-($c_4$) $Ni_2Mn_{1.5-x}Cu_xSn_{0.5}$ alloys.

In the $Ni_2Mn_{1.5-x}Cu_xSn_{0.5}$ alloys, the austenite exhibits a reduction in *a*, primarily due to the smaller atomic radius of Cu (1.28 Å) compared to Mn (1.32 Å), as depicted in Fig. 10(c_1). For the 4O martensite, with increasing Cu content *x*, *a* remains relatively constant, while *b* and *c* exhibit slight increases and decreases, respectively. For the NM martensite (Fig. 10(c_3)), *a* gradually increases, and

c decreases, resulting in a diminished value of |*c*/*a*-1|. This can be used to predict a decrease in the T_M.

In the Ni-Mn-Sn-Z*x* (*x* = 0~0.375) alloys, the transformation from austenite to 4O or NM martensite induces notable volume contraction due to the distinct volumes of austenite and martensites, as shown in Fig. 10(a_4)-(c_4). For the Fe-doped alloys, the volume contraction (△V) during martensitic transformation does not change significantly compared to undoped alloys (Fig. 10(a_4)). However, Co-doped alloys display a substantial and more pronounced contraction during martensitic transformation, exceeding that in ternary Ni-Mn-Sn alloys. Conversely, for the Cu-doped alloys, the △V during martensitic transformation is consistently smaller than that of the undoped Ni-Mn-Sn alloys, reaching its minimum at a Cu content of 0.25.

As is well-known, during the martensitic transformation, changes in both lattice parameters and unit cell volume change, alter interactions between atoms. This leads to an increase in frictional resistance at the phase transition interface, resulting in a significant $\triangle T_{Hys}$ during the first-order phase transition. Li *et al* experimentally observed that the △V is larger when *x* = 6 compared to *x* =5 in the $Mn_{50}Ni_{42-x}Co_xSn_8$ alloy, and they noted that an increase in the Co doping content leads to a corresponding increase in $\triangle T_{Hys}$[65,66]. Therefore, the $\triangle T_{Hys}$ can be qualitatively described by the △V during the phase transition. Based on the results of the first-principles calculations, we can predict that Cu doping can reduce the $\triangle T_{Hys}$ in Ni-Mn-Sn alloys. Particularly, around the Cu content of *x* = 0.25 for the $Ni_2Mn_{1.5-x}Cu_xSn_{0.5}$ alloys, the $\triangle T_{Hys}$ is minimized. This reduction is conducive to decreasing magnetic hysteresis losses and thus enhancing the reversibility of the magnetocaloric effect.

3.5 Electronic Structure

To further elucidate the origin of the physical properties related to the martensitic transformation and magnetic properties, Fig. 11 presents the total density of states (TDOS) for the austenite, 4O and NM martensites in the different alloy systems. A common feature in the spin-down TDOS of the four alloys is the presence of prominent peaks near the Fermi level (E_F) in the austenite, whereas the peaks transition into flat or even pseudo-gap near the E_F in the 4O and NM martensites. This observation signifies that the alloys have undergone the band Jahn-Teller effect[67], leading to martensitic

transformation, thereby lowering the total energy of the alloy and forming a more stable martensite.

Furthermore, the spin-up TDOS of austenite in the four alloys displays two obvious peaks at approximately -3 eV and -1 eV, which are primarily attributed to the strong 3*d* electronic interactions between Ni and Mn atoms. Unlike the other alloys, the spin-down TDOS of the $Ni_{1.875}Co_{0.125}Mn_{1.5}Sn_{0.5}$ alloy exhibits a pseudo-gap in the energy range of -0.5 to -1 eV, indicating the presence of strong bonding interactions between the atoms, as shown in Fig. 11(c). To further explore the underlying reason for bond formation, we calculated the partial density of states (PDOS) for this alloy, as shown in Fig. 12(a). This analysis reveals that the resonance between the minority electronic states of Ni and Co near the pseudogap is more pronounced than that between Ni and other atoms. This implies that the bond formation is primarily a result of hybridization between the minority electronic states of Ni and Co.

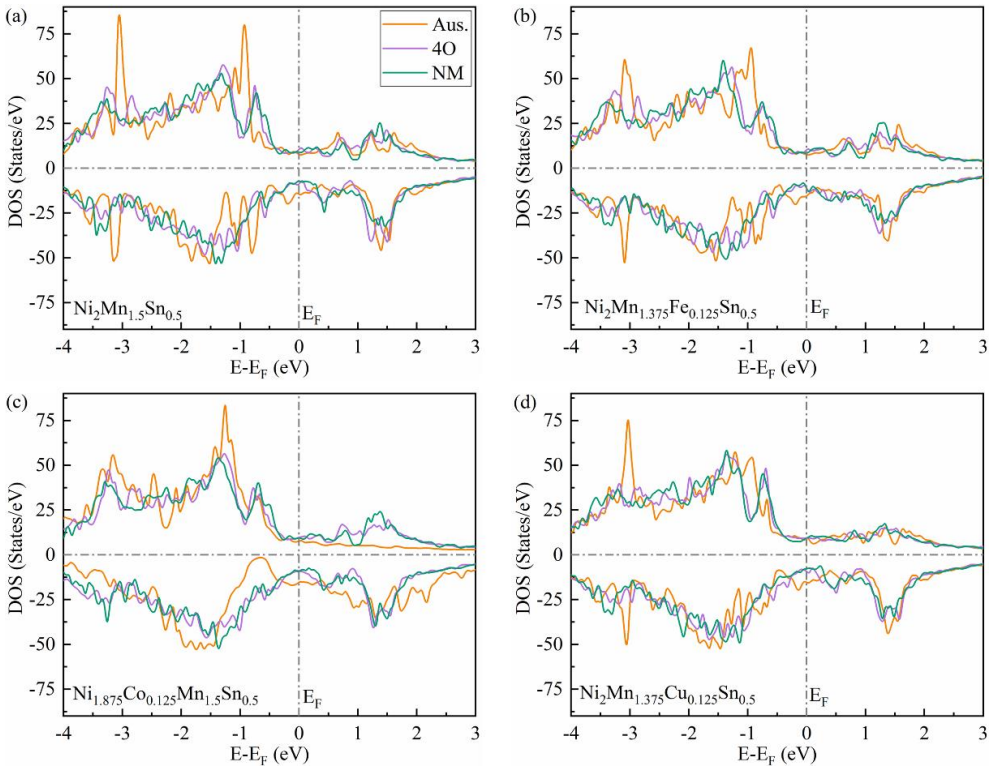

Fig. 11. TDOS near E_F of (a) $Ni_2Mn_{1.5}Sn_{0.5}$, (b) $Ni_2Mn_{1.375}Fe_{0.125}Sn_{0.5}$, (c) $Ni_{1.875}Co_{0.125}Mn_{1.5}Sn_{0.5}$, and (d) $Ni_2Mn_{1.375}Cu_{0.125}Sn_{0.5}$ alloys. E_F stands for zero energy.

To compare the electronic structure of the two magnetic states of austenite in the $Ni_2Mn_{1.5-x}Cu_xSn_{0.5}$ alloys when the Cu content is 0.25 and 0.375 respectively, we conducted calculations for the TDOS and PDOS of the austenite, as shown in Fig. 12(b) and (c). The total magnetic moment of these alloys is determined by the difference in the total number of electrons with spin-up and spin-

down below the Fermi level ($\triangle N$). The $\triangle N$ of x = 0.25 and x = 0.375 alloys are 15.663 and 34.643 electrons respectively. The increase in the electron number difference leads to an increase in the total magnetic moment, which is the fundamental reason for the change of the magnetism.

Moreover, it can be seen from Fig. 12(c) that in the $Ni_2Mn_{1.25}Cu_{0.25}Sn_{0.5}$ alloy (red line), the spin-up electrons of Mn_{Mn} are mainly distributed below the E_F, and the spin-down electrons are mainly distributed above the E_F, while the distribution of Mn_{Sn} is exactly the opposite, indicating that the magnetic moments of Mn_{Mn} and Mn_{Sn} are arranged antiparallel. In the $Ni_2Mn_{1.125}Cu_{0.375}Sn_{0.5}$ alloy (blue line), the spin direction of the Mn_{Sn} 3*d* state has changed, and the magnetic moments of Mn_{Mn} and Mn_{Sn} atoms become parallel, resulting in an enhancement of the total magnetic moment. Furthermore, the 3*d* states of Ni and Cu atoms are nearly fully occupied and exhibit high symmetry below the E_F, indicating that the magnetic moments of Ni and Cu atoms are relatively small. In contrast, for the Mn_{Mn} atoms, the 3*d* states with spin-up are half occupied, while the number of electrons occupied in the spin-down orbitals decreases below the E_F. This low-symmetry distribution for the density of states suggests that Mn atoms possess a larger magnetic moment, consistent with the atomic magnetic moment results presented in Section 3.4.

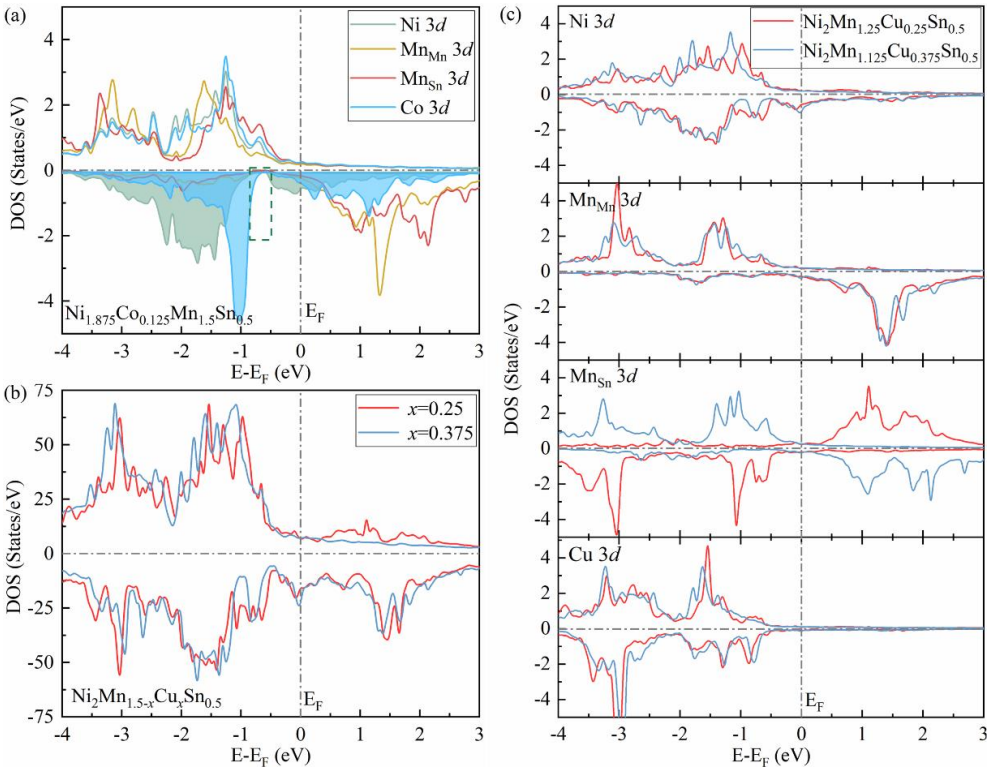

Fig. 12. (a) PDOS near E_F of $Ni_{1.875}Co_{0.125}Mn_{1.5}Sn_{0.5}$ alloy, (b) TDOS and (c) PDOS near E_F of $Ni_2Mn_{1.5-x}Cu_xSn_{0.5}$ (x = 0.25, 0.375) alloys. E_F stands for zero energy.

4 Conclusion

In this work, a comprehensive investigation including the phase stability, martensitic transformation, mechanical properties, and magnetic properties of the $Ni_2Mn_{1.5-x}Fe_xSn_{0.5}$, $Ni_{2-x}Co_xMn_{1.5}Sn_{0.5}$, and $Ni_2Mn_{1.5-x}Cu_xSn_{0.5}$ alloys was conducted by the first-principles calculations. The key results are outlined as follows:

(1) Fe and Co atoms preferentially occupy the sublattice of the Mn_{Mn} and Ni atoms, respectively; Cu atoms directly substitute for the Mn_{Sn} atoms or display indirect substitution by first occupying the sublattice of the Sn atoms, thereby forcing Sn atoms to occupy the Mn_{Sn} sublattice.

(2) According to the results of formation energy, the possible martensitic transformation path can be determined as: $Aus.^{FIM}\leftrightarrow 4O^{FIM}\leftrightarrow NM^{FIM}$ ($0 \le x \le 0.375$) for the $Ni_2Mn_{1.5-x}Fe_xSn_{0.5}$ alloys; $Aus.^{FIM}\leftrightarrow 4O^{FIM}\leftrightarrow NM^{FIM}$ ($0 \le x < 0.125$), $Aus.^{FIM/FM}\leftrightarrow 4O^{FIM}\leftrightarrow NM^{FIM}$ ($x = 0.125$), $Aus.^{FM}\leftrightarrow 4O^{FIM}\leftrightarrow NM^{FIM}$ ($0.125 < x < 0.375$), and $Aus.^{FM}\leftrightarrow NM^{FIM}$ ($x = 0.375$) for the $Ni_{2-x}Co_xMn_{1.5}Sn_{0.5}$ alloys; $Aus.^{FIM}\leftrightarrow 4O^{FIM}\leftrightarrow NM^{FIM}$ ($0 \le x < 0.375$) and $Aus.^{FM/FIM}\leftrightarrow 4O^{FIM}\leftrightarrow NM^{FIM}$ ($x = 0.375$) for the $Ni_2Mn_{1.5-x}Cu_xSn_{0.5}$ alloys. From the perspective of energy difference ($\triangle E_{Aus.-NM}$ and $\triangle E_{Aus.-4O}$), explain the underlying reasons for the increase in T_m increases with the increase in Fe content and the decrease with the increase in Co and Cu content.

(3) The analysis of mechanical properties demonstrates that the austenites exhibit higher plastic toughness compared to the 4O and NM martensites in both the matrix and various alloying systems. Fe or Cu doping increases the B/G, C^p, and v values of the austenite, enhancing the alloy's plasticity and toughness. In contrast, Co doping diminishes the toughness of austenite while increasing its stiffness.

(4) In the $Ni_2Mn_{1.5-x}Fe_xSn_{0.5}$ alloys, the total magnetic moments of austenite, 4O and NM martensites decrease as Fe content increases. For the $Ni_{2-x}Co_xMn_{1.5}Sn_{0.5}$ alloys, the total magnetic moments of austenite significantly increase with higher Co content, while the total magnetic moments of 4O and NM martensites remain stable. The $Ni_2Mn_{1.5-x}Cu_xSn_{0.5}$ alloys show an increase in total magnetic moments for austenite, 4O and NM martensites with increasing Cu content. In all three alloy systems, the variation trend of the total magnetic moment in the FIM austenite, 4O and NM martensites corresponds to that of Mn moments. Whether in the FIM or FM state of the austenite, the variation trend of the total magnetic moment aligns with that of the Ni moments. Co-doping enhances

the $\triangle M$ in the alloys, suggesting that Ni-Mn-Sn-Co alloys hold the potential to exhibit significant MCE.

(5) The variation in lattice constants in the three systems is primarily associated with atomic radii and magnetic interactions between atoms. The introduction of Cu leads to a reduction in $\triangle V$, consequently lowering thermal hysteresis.

CRediT authorship contribution statement

Yu Zhang: Writing – original draft, Conceptualization, Data curation. **Jing Bai** and **Nicola Morley**: Writing – review & editing, Supervision, Data curation. **Keliang Guo**, **Dan Liu**, **Jianglong Gu**, **Qingshuang Ma**, and **Qiuzhi Gao**: Data curation and Formal analysis. **Yudong Zhang**, **Claude Esling**, **Xiang Zhao**, and **Liang Zuo**: Supervision and Methodology. All authors contributed to the general discussion.

Data availability

Data will be made available on request.

Declaration of Competing Interest

The authors declare that they have no known competing financial interests or personal relationships that could have appeared to influence the work reported in this paper.

Acknowledgments

This work is financially supported by the National Natural Science Foundation of China (Grant No. 51771044), the Natural Science Foundation of Hebei Province (No. E2019501061), the Performance subsidy fund for Key Laboratory of Dielectric and Electrolyte Functional Material Hebei (No. 22567627H), the Fundamental Research Funds for the Central Universities (No. N2223025), 2023 Hebei Provincial doctoral candidate Innovation Ability training funding project (CXZZBS2023165), and the Programme of Introducing Talents of Discipline Innovation to Universities 2.0 (the 111 Project of China 2.0, No. BP0719037). Thanks to the support of the Shanxi Supercomputing Center of China, the calculations for this work were performed on TianHe-2. This project is supported by the China Scholarship Council (CSC).

References

[1] Y. Sutou, Y. Imano, N. Koeda, T. Omori, R. Kainuma, K. Ishida, K. Oikawa, Magnetic and

martensitic transformations of NiMnX (X=In, Sn, Sb) ferromagnetic shape memory alloys, Appl. Phys. Lett. 85 (2004) 4358-4360.

[2] R. Kainuma, Y. Imano, W. Ito, Y. Sutou, H. Morito, S. Okamoto, O. Kitakami, K. Oikawa, A. Fujita, T. Kanomata, K. Ishida, Magnetic-field-induced shape recovery by reverse phase transformation, Nature 439 (2006) 957-960.

[3] H.E. Karaca, I. Karaman, B. Basaran, Y. Ren, Y.I. Chumlyakov, H.J. Maier, Magnetic field-induced phase transformation in NiMnCoIn magnetic shape-memory alloys-A new actuation mechanism with large work output, Adv. Funct. Mater. 19 (2009) 983-998.

[4] N.M. Bruno, C. Yegin, I. Karaman, J.H. Chen, J.H. Ross, J. Liu, J.G. Li, The effect of heat treatments on $Ni_{43}Mn_{42}Co_4Sn_{11}$ meta-magnetic shape memory alloys for magnetic refrigeration, Acta. Mater. 74 (2014) 66-84.

[5] J.A. Monroe, I. Karaman, B. Basaran, W. Ito, R.Y. Umetsu, R. Kainuma, K. Koyama, Y.I. Chumlyakov, Direct measurement of large reversible magnetic-field-induced strain in Ni-Co-Mn-In metamagnetic shape memory alloys, Acta. Mater. 60 (2012) 6883-6891.

[6] D.M. Liu, Z.H. Nie, G. Wang, Y.D. Wang, D.E. Brown, J. Pearson, P.K. Liaw, Y. Ren, In-situ studies of stress- and magnetic-field-induced phase transformation in a polymer-bonded Ni-Co-Mn-In composite, Mater. Sci. Eng. A. 527 (2010) 3561-3571.

[7] T. Krenke, E. Duman, M. Acet, E.F. Wassermann, X. Moya, L. Mañosa, A. Planes, Inverse magnetocaloric effect in ferromagnetic Ni-Mn-Sn alloys, Nat. Mater. 4 (2005) 450-454.

[8] Z.B. Li, S.Y Dong, Z.Z. Li, B. Yang, F. Liu, C.F. Sánchez-Valdés, J.L. Sánchez Llamazares, Y.D. Zhang, C. Esling, X. Zhao, L. Zuo, Giant low-field magnetocaloric effect in Si alloyed Ni-Co-Mn-In alloys, Scripta. Mater. 159 (2019) 113-118.

[9] Z.B. Li, W. Hu, F.H. Chen, M.G. Zhang, Z.Z. Li, B. Yang, X. Zhao, L. Zuo, Large magnetoresistance in a directionally solidified $Ni_{44.5}Co_{5.1}Mn_{37.1}In_{13.3}$ magnetic shape memory alloy, J. Magn. Magn. Mater. 452 (2018) 249-252.

[10] S.Y. Yu, L. Ma, G.D. Liu, Z.H. Liu, J.L. Chen, Z.X. Cao, G.H. Wu, B. Zhang, X.X. Zhang, Magnetic field-induced martensitic transformation and large magnetoresistance in NiCoMnSb alloys, Appl. Phys. Lett. 90 (2007) 242501.

[11] M. Ye, A. Kimura, Y. Miura, M. Shirai, Y.T. Cui, K. Shimada, H. Namatame, M. Taniguchi, S.

Ueda, K. Kobayashi, R. Kainuma, T. Shishido, K. Fukushima, T. Kanomata, Role of electronic structure in the martensitic phase transition of $Ni_2Mn_{1+x}Sn_{1-x}$ studied by Hard-X-Ray photoelectron spectroscopy and ab initio calculation, Phys. Rev. Lett. 104 (2010) 176401.

[12] Y.D. Zhu, H.C. Xuan, J.C. Su, F.H. Chen, K.W. Zhang, P.D. Han, J.W. Qiao, Large elastocaloric effect in as-cast Ni-Mn-Sn-Fe ferromagnetic shape memory alloys, Phys. Lett. A. 451 (2022) 128374.

[13] Z.G. Wu, J.P. Guo, Z.W. Liang, Y.J. Zhang, X.J. Ye, J.S. Zhang, Y.C. Li, Y.N. Liu, H. Yang, Room temperature metamagnetic transformation of a tough dual-phase Ni-Mn-Sn-Fe ferromagnetic shape memory alloy, J. Alloy. Compd. 829 (2020) 154606.

[14] X.X. Zhang, H.H. Zhang, M.F. Qian, L. Geng, Enhanced magnetocaloric effect in Ni-Mn-Sn-Co alloys with two successive magnetostructural transformations, Sci. Rep. 8 (2018) 8235.

[15] Z.D. Han, D.H. Wang, B. Qian, J.F. Feng, X.F. Jiang, Y.W. Du, Phase transitions, magnetocaloric effect and magnetoresistance in Ni-Co-Mn-Sn ferromagnetic shape memory alloy, Jpn. J. Appl. Phys. 49 (2010) 010211.

[16] J.M. Wang, C. B. Jiang, A single-phase wide-hysteresis shape memory alloy $Ni_{50}Mn_{25}Ga_{17}Cu_8$, Scripta. Mater. 62 (2010) 298-300.

[17] J.M. Wang, H.Y. Bai, C.B. Jiang, Y. Li, H.B. Xu, A highly plastic $Ni_{50}Mn_{25}Cu_{18}Ga_7$ high-temperature shape memory alloy, Mater. Sci. Eng. A. 527 (2010) 1975-1978.

[18] Z.B. Li, J.J. Yang, D. Li, Z.Z. Li, B. Yang, H.L. Yan, C.F. Sánchez-Valdés, J.L. Sánchez Llamazares, Y.D. Zhang, Claude Esling, X. Zhao, L. Zuo, Tuning the reversible magnetocaloric effect in Ni-Mn-In-based alloys through Co and Cu co-doping, Adv. Electron. Mater. 5 (2019) 1800845.

[19] S. Saritaş, M. Kaya, I. Dinçer, Y. Elerman, The structural, magnetic, and magnetocaloric properties of $Ni_{43}Mn_{46-x}Cu_xIn_{11}$ (x=0, 0.9, 1.3, and 2.3) Heusler alloys, Metall. Mater. Trans. A. 48 (2017) 5068-5074.

[20] A. Ghotbi Varzaneh, P. Kameli, T. Amiri, K.K. Ramachandran, A. Mar, I. Abdolhosseini Sarsari, J.L. Luo, T.H. Etsell, H. Salamati, Effect of Cu substitution on magnetocaloric and critical behavior in $Ni_{47}Mn_{40}Sn_{13-x}Cu_x$ alloys, J. Alloy. Compd. 708 (2017) 34-42.

[21] Y. Li, W. Sun, D.W. Zhao, H. Xu, J. Liu, An 8 K elastocaloric temperature change induced by

1.3% transformation strain in $Ni_{44}Mn_{45-x}Sn_{11}Cu_x$ alloys, Scripta. Mater. 130 (2017) 278-282.

[22] E. Pagounis, R. Chulist, M.J. Szczerba, M. Laufenberg, Over 7% magnetic field-induced strain in a Ni-Mn-Ga five-layered martensite, Appl. Phys. Lett. 105 (2014) 052405.

[23] V.A. Chernenko, E. Villa, D. Salazar, J.M. Barandiaran, Large tensile superelasticity from intermartensitic transformations in $Ni_{49}Mn_{28}Ga_{23}$ single crystal, Appl. Phys. Lett. 108 (2016) 071903.

[24] A. Sozinov, N. Lanska, A. Soroka, W. Zou, 12% magnetic field-induced strain in Ni-Mn-Ga-based non-modulated martensite, Appl. Phys. Lett. 102 (2013) 021902.

[25] R. Chulist, P. Czaja, On the role of atomic shuffling in the 4O, 4M and 8M martensite structures in Ni-Mn-Sn single crystal, Scripta. Mater. 189 (2020) 106-111.

[26] C.Q. Lin, Dissertation for doctoral degree, Northeastern University, Shenyang, 2021.

[27] G. Kresse, D. Joubert, From ultrasoft pseudopotentials to the projector augmented-wave method, Phys. Rev. B. 59 (1999) 1758-1775.

[28] J. Hafner, Atomic-scale computational materials science, Acta. Mater. 48 (2000) 71-92.

[29] P.E. Blöchl, Projector augmented-wave method, Phys. Rev. B. 50 (1994) 17953-17979.

[30] G. Kern, G. Kresse, J. Hafner, Ab initio calculation of the lattice dynamics and phase diagram of boron nitride, Phys. Rev. B. 59 (1999) 8551-8559.

[31] J.P. Perdew, K. Burke, M. Ernzerhof, Generalized gradient approximation made simple, Phys. Rev. Lett. 77 (1996) 3865-3868.

[32] C.Q. Lin, H.L. Yan, Y.D. Zhang, C. Esling, X. Zhao, L. Zuo, Crystal structure of modulated martensite and crystallographic correlations between martensite variants of $Ni_{50}Mn_{38}Sn_{12}$ alloy, J. Appl. Cryst. 49 (2016) 1276-1283.

[33] S. Özdemir Kart, M. Uludoğan, I. Karaman, T. Çağın, DFT studies on structure, mechanics and phase behavior of magnetic shape memory alloys: Ni_2MnGa, Phys. stat. sol. (a) 205 (2008) 1026-1035.

[34] The Munich SPR-KKR package, version 8.6, H. Ebert et al, https://www.ebert.cup.uni-muenchen.de/sprkkr.

[35] H. Ebert, D. Köedderitzsch, J. Minár, Calculating condensed matter properties using the KKR-Green's function method—recent developments and applications, Rep. Prog. Phys. 74 (2011)

096501.

[36] A. Ghosh, K. Manda, Effect of structural disorder on the magnetocaloric properties of Ni-Mn-Sn alloy, Appl. Phys. Lett. 104 (2014) 031905.

[37] C.H. Huang, Y. Wang, Z. Tang, X.Q. Liao, S. Yang, X.P. Song, Influence of atomic ordering on elastocaloric and magnetocaloric effects of a Ni-Cu-Mn-Ga ferromagnetic shape memory alloy, J. Alloy. Compd. 630 (2015) 244-249.

[38] V.V. Sokolovskiy, V.D. Buchelnikov, M.A. Zagrebin, P. Entel, S. Sahoo, M. Ogura, First-principles investigation of chemical and structural disorder in magnetic $Ni_2Mn_{1+x}Sn_{1-x}$ Heusler alloys, Phys. Rev. B. 86 (2012) 134418.

[39] C.M. Li, H.B. Luo, Q.M. Hu, R. Yang, B. Johansson, L. Vitos, Role of magnetic and atomic ordering in the martensitic transformation of Ni-Mn-In from a first-principles study, Phys. Rev. B. 86 (2012) 214205.

[40] C.O. Aguilar-Ortiz, D. Soto-Parra, P. Álvarez-Alonso, P. Lázpita, D. Salazar, P.O. Castillo-Villa, H. Flores-Zúñiga, V.A. Chernenko, Influence of Fe doping and magnetic field on martensitic transition in Ni-Mn-Sn melt-spun ribbons, Acta. Mater. 107 (2016) 9-16.

[41] A. Deltell, Abd El-Moez A. Mohamed, P. Álvarez-Alonso, M. Ipatov, J.P. Andrés, J.A. González, T. Sánchez, A. Zhukov, M.L. Escoda, J.J. Suñol, R. López Antón, Martensitic transformation, magnetic and magnetocaloric properties of Ni-Mn-Fe-Sn Heusler ribbons, J. Mater. Res. Technol. 12 (2021) 1091-1103.

[42] H.S. Liu, C.L. Zhang, Z.D. Han, H.C. Xuan, D.H. Wang, Y.W. Du, The effect of Co doping on the magnetic entropy changes in $Ni_{44-x}Co_xMn_{45}Sn_{11}$ alloys, J. Alloy. Compd. 467 (2009) 27-30.

[43] F.S. Liu, Q.B. Wang, S.P. Li, W.Q. Ao, J.Q. Li, Effect of Co substitution on the martensitic transformation and magnetocaloric properties of $Ni_{50}Mn_{35-x}Co_xSn_{15}$, Powder. Diffr. 28 (2013) S22-S27.

[44] C. Jing, Y.J. Yang, Z. Li, X.L. Wang, B.J. Kang, S.X. Cao, J.C. Zhang, J. Zhu, B. Lu, Tuning martensitic transformation and large magnetoresistance in $Ni_{50-x}Cu_xMn_{38}Sn_{12}$ Heusler alloys, J. Appl. Phys. 113 (2013) 173902.

[45] R. Das, S. Sarma, A. Perumal, A. Srinivasan, Effect of Co and Cu substitution on the magnetic entropy change in $Ni_{46}Mn_{43}Sn_{11}$ alloy, J. Appl. Phys. 109 (2011) 07A901.

[46] K. Zhang, C.L. Tan, E.J. Guo, Z.C. Feng, J.C. Zhu, Y.X. Tong, W. Cai, Simultaneous tuning of martensitic transformation behavior, magnetic and mechanical properties in Ni-Mn-Sn magnetic alloy by Cu doping, J. Mater. Chem. C. 6 (2018) 5228-5238.

[47] J.L. Ouyang, Y. Tian, H.B. Xiao, Y.K. Zhang, Magnetic properties, martensitic transformations and magnetocaloric performances in $Ni_{44}Mn_{45-x}Fe_xSn_{11}$ (x=0-3) Heusler alloys, Mater. Chem. Phys. 273 (2021) 125150.

[48] B. Gao, J. Shen, F.X. Hu, J. Wang, J.R. Sun, B.G. Shen, Magnetic properties and magnetic entropy change in Heusler alloys $Ni_{50}Mn_{35-x}Cu_xSn_{15}$, Appl. Phys. A. 97 (2009) 443-447.

[49] D.Y. Cong, S. Roth, M. Pötschke, C. Hürrich, L. Schultz, Phase diagram and composition optimization for magnetic shape memory effect in Ni-Co-Mn-Sn alloys, Appl. Phys. Lett. 97 (2010) 021908.

[50] F. Mouhat, F.X. Coudert, Necessary and sufficient elastic stability conditions in various crystal systems, Phys. Rev. B. 90 (2014) 224104.

[51] T. Roy, M.E. Gruner, P. Enter, A. Chakrabarti, Effect of substitution on elastic stability, electronic structure and magnetic property of Ni-Mn based Heusler alloys: An ab initio comparison, J. Alloy. Compd. 632 (2015) 822-829.

[52] S. Ghosh, S. Ghosh, Understanding the origin of the magnetocaloric effects in substitutional Ni-Mn-Sb-Z (Z=Fe, Co, Cu) compounds: Insights from first-principles calculations, Phys. Rev. B. 101 (2020) 024109.

[53] A. Marmier, Z.A.D. Lethbridge, R.I. Walton, C.W. Smith, S.C. Parker, K.E. Evans, ElAM: A computer program for the analysis and representation of anisotropic elastic properties, Comput. Phys. Commun. 181 (2010) 2101-2115.

[54] T. Roy, D. Pandey, A. Chakrabarti, Probing the possibility of coexistence of martensite transition and half-metallicity in Ni and Co-based full-Heusler alloys: An ab initio calculation, Phys. Rev. B. 93 (2016) 184102.

[55] B. Benichou, H. Bouchenafa, Z. Nabi, B. Bouabdallah, First-principles calculations to investigate the structural, mechanical, electronic, magnetic and thermodynamic characteristics of the full-Heusler alloys Pd_2MnSb, Pd_2MnIn, and $Pd_2MnSb_{1-x}In_x$ (x = 0.25, 0.5, 0.75), Comput. Condens. Matte. 32 (2022) e00697.

[56] Q. Mahmood, M. Yaseen, Bakhtiar Ul Haq, A. Larefd, A. Nazire, The study of mechanical and thermoelectric behavior of $MgXO_3$ (X = Si, Ge, Sn) for energy applications by DFT, Chem. Phys. 524 (2019) 106-112.

[57] D.G. Pettifor, D. Pettifor, Bonding and Structure of Molecules and Solids, Clarendon Press, Oxford, 1995, pp. 50-276.

[58] D.Y. Cong, W.X. Xiong, A. Planes, Y. Ren, L. Mañosa, P.Y. Cao, Z.H. Nie, X.M. Sun, Z. Yang. X.F. Hong, Y.D. Wang, Colossal elastocaloric effect in ferroelastic Ni-Mn-Ti alloys, Phys. Rev. Lett. 122 (2019) 255703.

[59] R.H. Baughman, J.M. Shacklette, A.A. Zakhidov, S. Stafström, Negative Poisson's ratios as a common feature of cubic metals, Nature 392 (1998) 362-365.

[60] G.J. Li, L. Xu, Z.H. Cao, A unified physical mechanism for martensitic phase transition and ductility in Ni-Mn-based ferromagnetic shape memory alloys: the case of Cu-doped Ni_2MnGa, J. Mater. Chem. C 11 (2023) 6173-6182.

[61] Y. Feng, J.H. Sui, Z.Y. Gao, W. Cai, Investigation of martensitic transformation and mechanical properties of the $Ni_{50}Mn_{37-x}Sn_{13}Fe_x$ (x=0, 2, 5, 10) alloys, Int. J. Mod. Phys. B. 23 (2009) 1803-1808.

[62] C.M. Li, H.B. Luo, Q.M. Hu, R. Yang, B. Johansson, L. Vitos, Site preference and elastic properties of Fe-, Co-, and Cu-doped NiMnGa shape memory alloys from first principles, Phys. Rev. B. 84 (2011) 024206.

[63] A. Kundu, S. Ghosh, S. Ghosh, Effect of Fe and Co substitution on the martensitic stability and the elastic, electronic, and magnetic properties of Mn_2NiGa: Insights from ab initio calculations, Phys. Rev. B. 96 (2017) 174107.

[64] C.M. Li, H.B. Luo, Q.M. Hu, R. Yang, B. Johansson, L. Vitos, First-principles investigation of the composition dependent properties of $Ni_{2+x}Mn_{1-x}Ga$ shape-memory alloys, Phys. Rev. B. 82 (2010) 024201.

[65] Y.W. Jiang, Dissertation for master's degree, Northeastern University, Shenyang, 2016.

[66] Z.B. Li, Y.W. Jiang, Z.Z. Li, C.F. Sánchez-Valdés, J.L. Sánchez Llamazares, B. Yang, Y.D. Zhang, C. Esling, X. Zhao, L. Zuo, Phase transition and magnetocaloric properties of $Mn_{50}Ni_{42-x}Co_xSn_8$ ($0\leq x\leq 10$) melt-spun ribbons, IUCrJ. 5 (2018) 54-66.

[67] S.R. Barman, S. Banik, A. Chakrabarti, Structural and electronic properties of Ni_2MnGa, Phys. Rev. B. 72 (2005) 184410.